The biogeochemical impact of glacial meltwater from Southwest Greenland

Katharine R. Hendry[1], Veerle A. I. Huvenne[2], Laura F. Robinson[1], Amber Annett[3], Marcus Badger[4], Allison W. Jacobel[5,6], Hong Chin Ng[1], Jacob Opher[7-9], Rebecca A. Pickering[10,11], Michelle L. Taylor[12], Stephanie L. Bates[1], Adam Cooper[3], Grace G. Cushman[5], Claire Goodwin[13], Shannon Hoy[14], George Rowland[1], Ana Samperiz[1,15], James A. Williams[15], Eric P. Achterberg[16], Carol Arrowsmith[17], J. Alexander Brearley[7], Sian F. Henley[18], Jeffrey W. Krause[10,11], Melanie J. Leng[17,19], Tao Li[1], Jerry F. McManus[5], Michael P. Meredith[7], Rupert Perkins[15], and E. Malcolm S. Woodward[20]

[1] School of Earth Sciences, University of Bristol, Wills Memorial Building, Queen's Road, Bristol, BS8 1RJ, UK

[2] National Oceanography Centre, University of Southampton Waterfront Campus, European Way, Southampton, SO14 3ZH, UK

[3] Ocean and Earth Science, University of Southampton, Waterfront Campus, European Way, Southampton, SO14 3ZH, UK

[4] School of Environment, Earth & Ecosystem Sciences, The Open University, Walton Hall, Milton Keynes, MK7 6AA, UK

[5] Lamont-Doherty Earth Observatory, Columbia University, 61 US-9W, Palisades, NY 10964, USA

[6] Environment and Society, Brown University, 85 Waterman Street, Providence, RI 02912, USA

[7] British Antarctic Survey, High Cross, Madingley Road, Cambridge, CB3 0ET, UK

[8] Centre for Ocean and Atmospheric Sciences, School of Environmental Sciences, University of East Anglia, Norwich Research Park, Norwich NR4 7TJ, UK

[9] Centre for Environment Fisheries and Aquaculture Science, Pakefield Road, Lowestoft, Suffolk NR33 0HT, UK

[10] Dauphin Island Sea Laboratory, 101 Bienville Boulevard, Dauphin Island, AL 36528, USA

[11] University of South Alabama, Mobile, AL, 36688, USA

[12] School of Biological Sciences, University of Essex, Wivenhoe Park, Colchester, CO4 3SQ, UK

[13] Huntsman Marine Science Centre, 1 Lower Campus Rd, Saint Andrews, NB E5B 2L7, Canada

[14] Center for Coastal & Ocean Mapping/Joint Hydrographic Center, Jere A. Chase Ocean Engineering Lab, 24 Colovos Road, Durham, New Hampshire 03824, USA
[15] School of Earth and Ocean Sciences, Cardiff University, Main Building, Park Place, Cardiff, CF10 3AT, UK
[16] GEOMAR Helmholtz Centre for Ocean Research, Kiel, Wischhofstraße 1-3, D-24148 Kiel, Germany
[17] NERC Isotope Geosciences Facility, British Geological Survey, Keyworth, Nottingham, NG12 3GG, UK
[18] School of GeoSciences, University of Edinburgh, James Hutton Road, Edinburgh, EH9 3FE, UK
[19] Centre for Environmental Geochemistry, School of Biosciences, Sutton Bonington Campus, University of Nottingham, Loughborough, LE12 5RD, UK.
[20] Plymouth Marine Laboratory, Prospect Place, The Hoe, Plymouth, PL1 3DH, UK
*Corresponding author: K.Hendry@bristol.ac.uk

Abstract

Biogeochemical cycling in high-latitude regions has a disproportionate impact on global nutrient budgets. Here, we introduce a holistic, multi-disciplinary framework for elucidating the influence of glacial meltwaters, shelf currents, and biological production on biogeochemical cycling in high-latitude continental margins, with a focus on the silica cycle. Our findings highlight the impact of significant glacial discharge on nutrient supply to shelf and slope waters, as well as surface and benthic production in these regions, over a range of timescales from days to thousands of years. Whilst biological uptake in fjords and strong diatom activity in coastal waters maintains low dissolved silicon concentrations in surface waters, we find important but spatially heterogeneous additions of particulates into the system, which are transported rapidly away from the shore. We expect the glacially-derived particles – together with biogenic silica tests – to be cycled rapidly through shallow sediments, resulting in a strong benthic flux of dissolved silicon. Entrainment of this benthic silicon into boundary currents may supply an important source of this key nutrient into the Labrador Sea, and is also likely to recirculate back into the deep fjords inshore. This study illustrates how geochemical and oceanographic analyses can be used together to probe further into modern nutrient cycling in this region, as well as the palaeoclimatological

approaches to investigating changes in glacial meltwater discharge through time, especially during periods of rapid climatic change in the Late Quaternary.

Keywords

Biogeochemistry, nutrients, glaciers, primary production, silica cycling

Highlights

- Novel multi-disciplinary approach to tracing freshwater and particle transport into boundary currents;
- Significant glacial inputs reach coastal waters and are transported rapidly offshore;
- Low surface water dissolved silicon concentrations maintained by diatom activity despite strong glacial and benthic supplies.

1. Introduction

The high-latitude regions are experiencing some of the most rapid environmental changes observed globally in recent decades. This is particularly true for the Arctic. Here, temperatures are rising twice as fast as the global mean, the Nordic Seas are warming at an accelerated rate (Alexeev, Walsh, Ivanov, Semenov & Smirnov, 2017), Arctic sea-ice is thinning and moving faster (Lindsay & Schweiger, 2015), and multi-year Arctic sea-ice is declining (Maslanik, Fowler, Stroeve, Drobot, Zwally et al., 2007), with significant implications for the interaction between the atmosphere and the oceans (Provost, Sennéchael, Miguet, Itkin, Rösel et al., 2017). The Greenland Ice Sheet (GrIS) is experiencing significant mass loss largely through surface melting but also via ice discharge at glacier fronts (Enderlin, Howat, Jeong, Noh, Van Angelen et al., 2014; Felikson, Bartholomaus, Catania, Korsgaard, Kjær et al., 2017; van den Broeke, Box, Fettweis, Hanna, Noël et al., 2017). This melting is likely to have a global impact: the North Atlantic receives freshwater from the Nordic Seas, GrIS, and the Canadian Arctic (Bamber, Tedstone, King, Howat, Enderlin et al., 2018), which influences the density structure, circulation, and stratification in regions where deep water-masses form; these represent a major component of ocean circulation that drives global fluxes of heat and freshwater (Carmack, Yamamoto-Kawai, Haine, Bacon, Bluhm et al., 2016; Proshutinsky, Dukhovskoy, Timmermans, Krishfield & Bamber, 2015; Yang, Dixon, Myers, Bonin, Chambers et al., 2016). In addition to freshwater budgets, there has been increasing focus on the role of glaciers and ice sheets in supplying organic material and inorganic nutrients to marine systems. There are significant fluxes of nutrients in GrIS runoff both in dissolved and particulate form, including nitrogen (Wadham, Hawkings, Telling, Chandler, Alcock et al., 2016), phosphate (Hawkings, Wadham, Tranter, Telling, Bagshaw et al., 2016), dissolved silicon (Hawkings, Wadham, Benning, Hendry, Tranter et al., 2017; Meire, Meire, Struyf, Krawczyk, Arendt et al., 2016), and iron (Bhatia, Kujawinski, Das, Breier, Henderson et al., 2013; Hawkings, Wadham, Tranter, Raiswell, Benning et al., 2014). The extent to which these nutrients reach the coastal oceans, and are subsequently advected or mixed from the continental shelves into the open oceans via boundary currents, is poorly constrained and a matter of debate (Hopwood, Bacon, Arendt, Connelly & Statham, 2015). Both dissolved nutrient and particulate dynamics are significantly impacted by circulation processes (Hopwood et al., 2015) and biological activity within glacially-influenced fjords. These regions could be a significant trap of dissolved

inorganic phases (Meire, Mortensen, Meire, Juul-Pedersen, Sejr et al., 2017), and have the potential to prevent the nutrient-rich glacial waters reaching the coastal seas. Despite this possibility, distal summer phytoplankton blooms have been detected off Southwest Greenland in association with glacial melt (Arrigo, van Dijken, Castelao, Luo, Rennermalm et al., 2017) and ecosystem models indicate sensitivity to meltwater input (Oliver, Luo, Castelao, van Dijken, Mattingly et al., 2018). An understanding of how natural resources – including fisheries, bird, and mammal stocks that are essential for food and encouraging tourism – will respond in the future to increasing anthropogenic stress on a regional and global scale relies on an understanding of foundational processes of these ecosystem services, including marine biogeochemistry and the sources and sinks of essential nutrients (Berthelsen, 2014; Meire et al., 2017; Weatherdon, Magnan, Rogers, Sumaila & Cheung, 2016).

The overarching goal of the Isotope Cycling in the Labrador Sea (ICY-LAB; icylab.wordpress.com) study is to understand the cycling of nutrients in the climatically critical but understudied regions of the Labrador Sea and Greenland fjords. The approach of ICY-LAB is to capture the whole biogeochemical system in these areas of marked environmental change using carefully planned field sampling strategies, with research expeditions to coastal Greenland and the open ocean Labrador Sea. The principal dataset was collected during an oceanic expedition on the RRS *Discovery* (DY081, July-August 2017), with the aim to investigate the influence of glacial meltwater on nutrient cycling in the shelf seas off SW Greenland. Particular focus was placed on the silica budget and how this is framed within the oceanographic and biological processes acting on the W Greenland margin. Uniquely, we combined a range of both traditional and novel methodologies to detect and trace meltwater and glacial material from the shelf across the slope, and to investigate the biogeochemical and biological impact of these inputs. Bringing these different approaches together is essential in these margin environments to obtain a full picture of biogeochemical cycling, providing a robust insight into the system over a range of spatial and temporal scales that are otherwise challenging to resolve (Figure 1).

2. Methods and materials

2.1. Fieldwork rationale

The data presented in this paper were collected during expedition DY081, centred on the coastal shelf and slope regions off Southwest Greenland. Model results indicate that this region is influenced by surface meltwater from the Western GrIS, in addition to a significant input of freshwater delivered from the Eastern GrIS via the strong East Greenland Current (EGC) (Luo, Castelao, Rennermalm, Tedesco, Bracco et al., 2016). The study locations were selected to represent this conduit to the open ocean for glacial runoff from the Western and Southwestern GrIS, which have been the focus of recent terrestrial studies carried out in collaboration with the Bristol Glaciology Centre (Hawkings, Hatton, Hendry, de Souza, Wadham et al., 2018; Hawkings et al., 2017). Full details of the oceanographic setting are given in Appendix A.

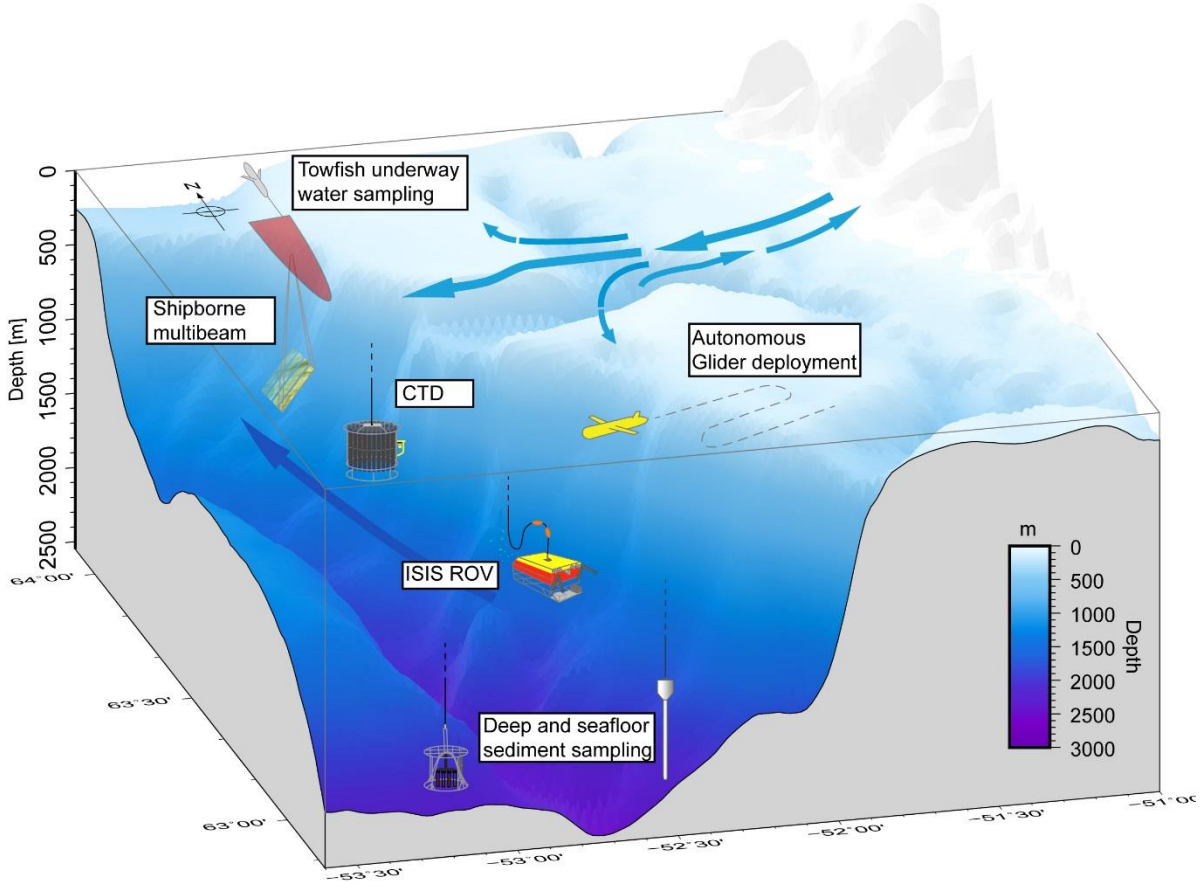

Figure 1: Summary figure showing the multi-discipline approach taken during expedition DY081 of project ICY-LAB.

We selected the main study location for the ICY-LAB project ("Gothåb (Nuuk) Trough", Figure 2a) to be adjacent to Nuuk, which has experienced increasing glacial run-off in recent years (Van As, Andersen, Petersen, Fettweis, Van Angelen et al., 2014). During DY081, Southern Greenland was strongly influenced by both icebergs and sea ice, but two sites ("Narsaq" and "Cape Farewell", Figure 2a) were still selected there for providing glacial troughs that could act as direct comparisons to the further north Nuuk site further north. Orphan Knoll, on the western margin of the Labrador Sea, was selected as a distal comparison site, and for complementary palaeoclimate, biological and habitat mapping studies (Figure 2a).

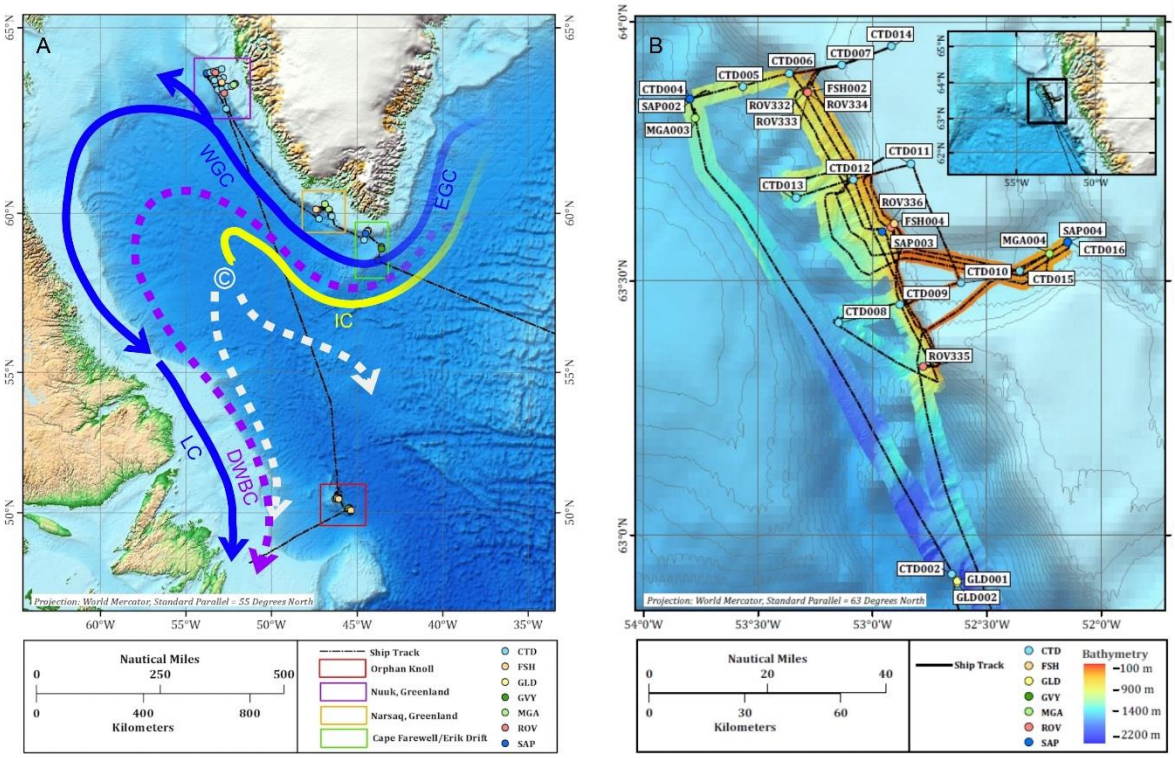

Figure 2: A) Map showing route and main working areas of expedition DY081. Produced in Mercator projection with a standard parallel of 55˚N. Arrows show the main current systems in the Labrador Sea: Irminger Current (IC in yellow), West and East Greenland Currents and Labrador Current (WGC, EGC, LC in blue), and the Deep Western Boundary Current (DWBC). Cold, deep polar overflow waters are represented by the purple arrow. The main site of deep-water convection is marked by C, and represented by white arrows. B) Map of Nuuk grid location with ship track, bathymetry and station locations. Produced in Mercator projection with a standard parallel of 63˚N.

The unique holistic observational approach we took is illustrated in Figure 1, and included (a) initial bathymetric mapping using acoustic methods (multibeam echosounders) to increase our understanding of the local terrain and to enable accurate planning of further

sampling activities; (b) characterisation of the water column structure using CTD casts and glider deployments; (c) sampling of surface and bottom waters for biogeochemical analyses using the CTD rosette and a trace metal clean towfish; (d) sampling of seabed sediments using a megacorer (for geochemical studies of pore waters) and gravity corer (for palaeoceanographic investigations); (e) seabed observations and precision sampling for biological, palaeoceanographic and sedimentological studies using a work-class scientific ROV.

2.2. On-board methodologies and additional laboratory techniques

2.2.1. Mapping and acoustics

During DY081, multiple acoustic systems were deployed on the ship (e.g. EM122 multibeam echosounder (12 kHz); EM710 multibeam echosounder; SBP120 sub-bottom echosounder (2.5 – 6.5 kHz)). These were coordinated via a K-Sync system to avoid interference and crosstalk.

Bathymetry data were processed on-board with the Caris HIPS & SIPS software v.8, using standard settings and procedures (data import, navigation and attitude check, application of a “zero tide”, gridding into a 25 mx25 m pixel BASE surface). Backscatter data were processed with Fledermaus FMGT, again using default settings.

2.2.2. Physical oceanography

High-resolution water column studies surrounding the prominent glacial Gothåb (Nuuk) Trough were carried out utilising both a grid of Conductivity Temperature Depth (CTD) casts and the deployment of two 1000m-rated Slocum gliders (Figure 2). CTD casts were also used at the south Greenland and Orphan Knoll study sites. Hydrographic analysis enabled characterization of the water column structure in each study location, specifically to locate and quantify the freshwater inputs at the Greenland sites. Salinity was calibrated using bottle samples collected at discrete depths. After laboratory calibration of these samples, no drift corrections were required. Overall errors for temperature were 0.0006 °C (based on laboratory calibration) and 0.002 for salinity. Prior to analysis, data from these stations were gridded to a vertical and horizontal resolution of 10 m and 6 km respectively.

Vessel Mounted Acoustic Doppler Current Profilers (VMADP at 75 and 150kHz; Teledyne RD instruments) were secured onto the drop keel in surface waters near the centre-line and

beneath the *RRS Discovery*, and used to measure the horizontal current velocity profile. Bottom tracking data were only collected from the 150 kHz instrument intermittently between 18th July and 24th July 2017 while close to Nuuk. In addition, downward and upward looking lowered 300 kHz ADCPs (LADCPs) were mounted on the CTD rosette. LADCP data were processed using LDEO LADCP processing software version IX_8, run on Matlab. Full details of the other sensors attached to the CTD rosette and gliders can be found elsewhere (Hendry, 2017).

2.2.3. Biogeochemistry and chemical oceanography

2.2.3.1. Water column

Water column samples were collected using Niskin bottles attached to the CTD rosette (10L volume) and the Remotely Operated Vehicle (ROV) *Isis* (4 L volume), and via a trace-metal clean towfish. The towfish system comprised of a weighted titanium bodied fish lowered into the water at the stern and streamed as far from the ship as possible. When towed it was at approximately 2m depth, and water was pumped into the ship's labs through an ultra-clean pump and tubing. Trace-metal sampling was only carried out when the ship was moving at speeds greater than 0.5 knots in order to avoid contamination from the hull of the vessel. Four stand-alone pumps (SAPs) were also deployed at key locations to collect water column particles.

Samples of seawater were collected for inorganic macronutrients, water oxygen isotope composition ($\delta^{18}O$) and carbonate chemistry parameters (pH, alkalinity), which are used for investigating freshwater input in high-latitude regions (Hendry, Pyle, Barney Butler, Cooper, Fransson et al., 2018; Meredith, Brandon, Wallace, Clarke, Leng et al., 2008; Thomas, Shadwick, Dehairs, Lansard, Mucci et al., 2011). Phytoplankton pigments were analysed on board, and compared to sensor-derived fluorescence data, to assess algal standing stocks in relation to meltwater input. Full details of sampling methods and laboratory techniques are available in Appendix B.

2.2.3.2. Diatom productivity

Biogenic silica ($bSiO_2$) production (i.e. diatom productivity) analyses were done using radioisotope ^{32}Si as detailed in Krause, Brzezinski and Jones (2011). Briefly, samples were collected within the euphotic zone (sample depths based on light and relative to irradiance

just below the surface) and dispensed into acid-cleaned 125 mL polycarbonate bottles. 322 Bq of $^{32}Si(OH)_4$ was added to each sample, and bottles were incubated on deck in surface-seawater-cooled incubators covered with neutral density screening to mimic the depth of collection. After incubation, samples were filtered through 1.2 µm pore size polycarbonate membrane filters. Particulate ^{32}Si activity was quantified using a GM-25 Multicounter (Risø DTU National Laboratory, Denmark) after the samples had aged into secular equilibrium with the short-lived daughter isotope, ^{32}P.

2.2.3.3. Radium isotopes

To investigate the fate of solutes sourced from benthic sediments or glacial meltwater, large-volume surface samples for radium (Ra) isotope analysis were collected from the trace-metal clean towfish system, both when the ship was underway (~2m water depth) and stationary (~5m water depth). A total of 200-300 L of seawater from a single sampling event were then passed through a plastic column holding MnO_2-coated acrylic fibre, which quantitatively binds Ra in the sample. The fibers and adsorbed Ra isotopes were then rinsed with deionized water (Milli-Q, Millipore), dried to an appropriate moisture content and loaded into a Ra Delayed Coincidence Counter (RaDeCC; Scientific Computer Instruments, USA) so as to quantify ^{223}Ra and ^{224}Ra content following the methods of Moore and Arnold (1996) and Moore (2008). Each sample was counted 4 times over ~4 months to determine the activities of excess ^{224}Ra and ^{223}Ra, above the activities supported by their parent isotopes in the water column (^{228}Th and ^{227}Ac, respectively). Detector efficiencies were determined and monitored regularly at sea and in the laboratory with standards (Annett, Henley, Van Beek, Souhaut, Ganeshram et al., 2013). Final reported activities have been corrected for any decay that occurred between sample collection and analysis, activity supported by parent isotopes, detector background, and efficiency.

2.2.3.4. Sediment-water interface

High-latitude ocean margin sediments are increasingly being recognised as an important source of inorganic nutrients and key elements (Henley, Jones, Venables, Meredith, Firing et al., 2018; Kuzyk, Gobeil, Goñi & Macdonald, 2017; Sherrell, Annett, Fitzsimmons, Roccanova & Meredith, 2018). To investigate the role of sediments in these glacially-influenced shelf and slope environments, we collected pore-fluid samples at coastal

Greenland and the Labrador Sea. Short sediment cores (≤40 cm) were acquired from the study area with a mega corer. Using Rhizon filters (0.15 µm, Rhizosphere Research Products), pore water was extracted from the sediment cores and filtered into syringes, and the samples were stored under cool conditions prior to analysis. Pore water dissolved silicon concentrations were analysed on-board and post-expedition using a V-1200 Vis spectrophotometer, employing a standard molybdate-blue methodology (using Hach Lange reagents). The samples were corrected for blank and calibrated against a ten-point curve that was developed using Si standards of known concentrations. In addition to mega-cores, we also employed ROV push cores to obtain short sediment cores for pore-fluid sampling, in regions where complex bathymetry or the presence of ice-rafted material precluded the use of a megacorer.

2.2.4. Palaeoclimate

Two samples types were collected for palaeoclimate research – fossil deep-sea corals and sediment cores. ROV operations were the primary tool for benthic biological and fossil coral collections using grab or suction devices. In addition, where large fossil coral graveyards were observed, a net was used to sample fossil corals. Gravity cores were also collected to obtain long-term records of changes in meltwater flux and iceberg dynamics over the Late Quaternary, thereby providing a longer-term temporal context to the broader data set. Megacores, collected primarily for biogeochemical studies, were also subsampled to provide core-top material that could potentially replace any sections lost from the gravity cores during retrieval.

2.3. Mass balance calculations

To calculate the freshwater mass balance in the study area, the seawater samples are presumed to comprise a mixture of three source water end-members: ocean, sea ice melt and meteoric water, which is assumed to be dominated by glacial discharge. The three end-member assumption enables quantification of the freshwater fractions via the following mass balance equations (Meredith, Heywood, Dennis, Goldson, White et al., 2001):

$$F_{ir} + F_{me} + F_{si} = 1$$

$$F_{ir}S_{ir} + F_{me}S_{me} + F_{si}S_{si} = S_{ms}$$

294 $$F_{ir}\delta_{ir} + F_{me}\delta_{me} + F_{si}\delta_{si} = \delta_{ms}$$

295

296 Where F_{ir}, F_{me}, F_{si} are the calculated fractions of Irminger Water, meteoric and sea ice melt
297 respectively (Irminger Water being the chosen ocean endmember), which sum to 1 by
298 definition. The result is clearly dependent on the exact choice of endmembers for salinity
299 (S_{ir}, S_{me}, S_{si}) and $\delta^{18}O$ (δ_{ir}, δ_{me}, δ_{si}) for the Irminger Water, meteoric and sea ice melt
300 respectively. S_{ms} and δ_{ms} are the measured salinity and $\delta^{18}O$ of each sample.
301 Properties for the sea ice melt and meteoric endmembers (Table 1) were based on values
302 reported in Dodd, Heywood, Meredith, Naveira-Garabato, Marca et al. (2009); Melling and
303 Moore (1995); Meredith et al. (2001); and the CTD observations from the DY081 research
304 cruise. Note that negative sea ice melt percentages reflect a net sea ice formation from the
305 water parcel sampled.

306

307 **3. Results**

308

309 EM-122 multibeam swath bathymetry datasets (e.g. Figure 2) are now published on
310 PANGAEA (doi: 10.1594/PANGAEA.892825). The full water column data from CTD profiles
311 and bottles (hydrography, oxygen isotopes, carbonate chemistry, macronutrients e.g. Figure
312 3) are published on PANGAEA (doi.pangaea.de/10.1594/PANGAEA.896544). Here we
313 present a subset of the results, focusing on characterisation of the silica cycle in the water
314 column and sediments.

315

316 **3.1. Silica cycling parameters in the water column and sediments**

317

318 *3.1.1. Water column macronutrients and pigments*

319 The nearshore macronutrient concentrations were typically low (< 11 μM nitrate, < 0.2
320 μM nitrite, < 0.75 μM phosphate and < 5 μM DSi in the upper 50 m of the water column)
321 reaching minima in the surface waters with lowest salinity and lowest $\delta^{18}O$ (an example of
322 which is given in Figure 3a, see also Appendix C). Sections of CTD macronutrient and
323 pigment bottle data from the Nuuk grid, integrated over the top 50m, reveal consistent
324 onshore-offshore trends (an example of which is given in Figure 3b, see also Appendix B).
325 Integrated macronutrient concentrations decreased towards shore concurrent with an

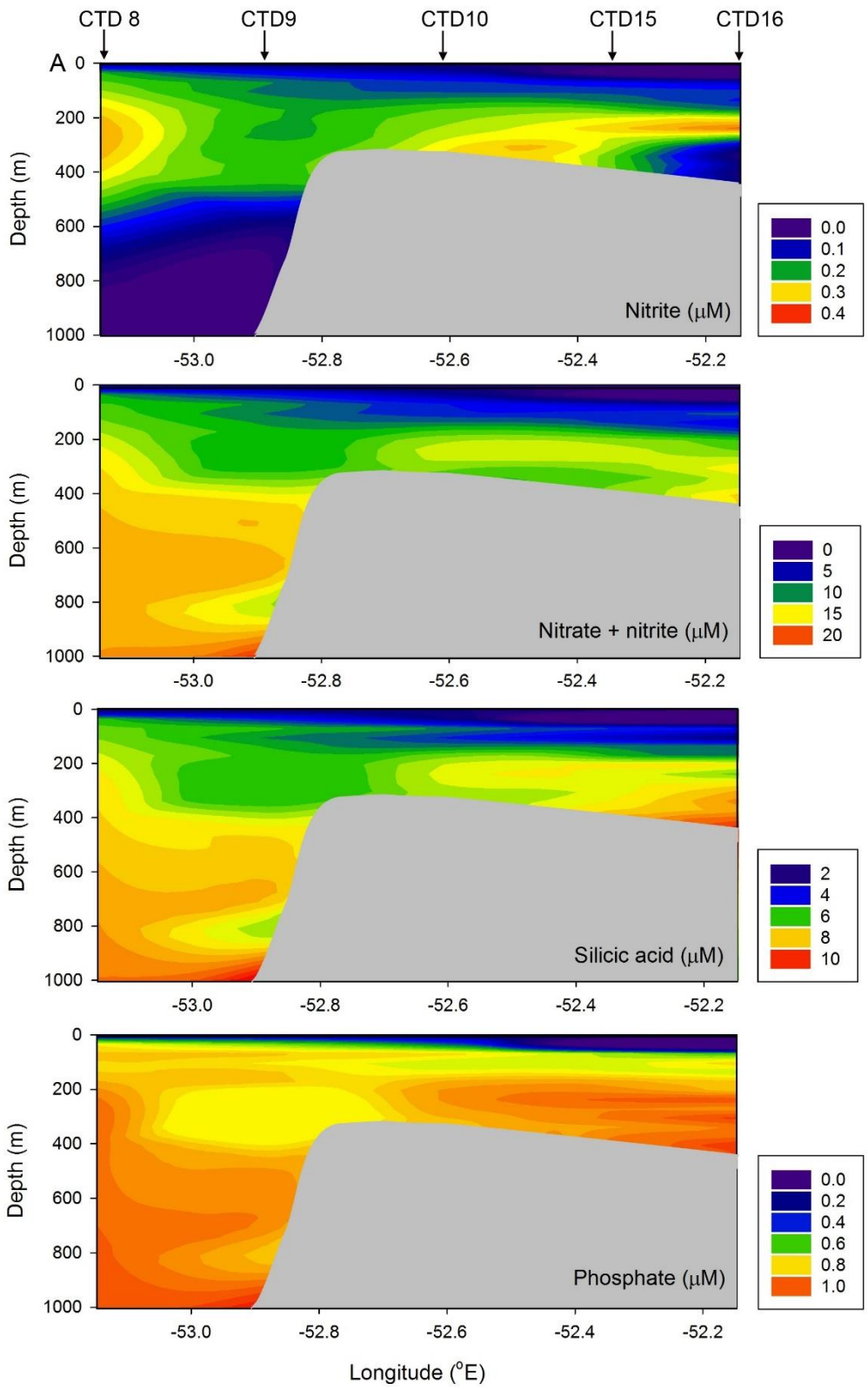
CTD 8
CTD9
CTD10
CTD15
CTD16
A
Depth (m)
0
200
400
600
800
1000
Nitrite (μM)
0.0
0.1
0.2
0.3
0.4
Nitrate + nitrite (μM)
0
5
10
15
20
Silicic acid (μM)
2
4
6
8
10
Phosphate (μM)
0.0
0.2
0.4
0.6
0.8
1.0
-53.0
-52.8
-52.6
-52.4
-52.2
Longitude (°E)

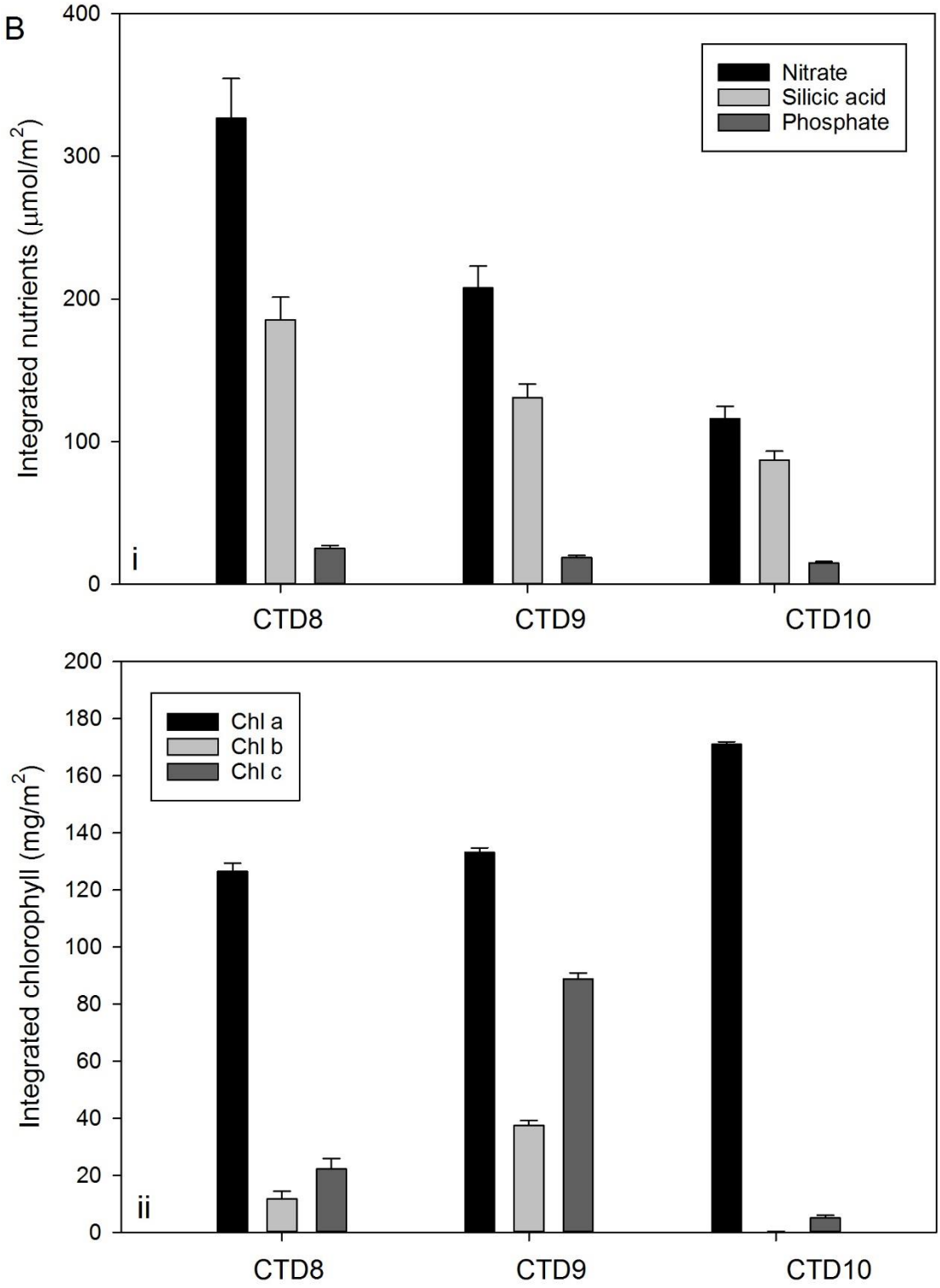

Figure 3: A) Example cross section of macronutrient concentrations from the Nuuk grid (from CTD 8 to CTD 16), showing (from top to bottom): nitrite, nitrate, silicic acid, and phosphate (all in µM). This section crosses the shelf break and occupied the prominent glacial trough, as shown in Figure 2.
B) Example cross section of integrated (top 50 m) macronutrient and algal pigment concentrations from the Nuuk grid (from CTD 8 to CTD 10, see Figure 2). i) Integrated macronutrients; ii) Integrated pigment concentrations. Error bars show propagated errors on integration calculation (±1SD).

increase in Si:N. Integrated Chl *a* increased towards shore, indicative that at least some of the macronutrient decrease is a result of biological uptake into biomass. However, the ratio of Chl *a*:Chl *c* peaked at the shelf break, and then decreased again towards shore, indicating a lower diatom proportional contribution to biomass in the same locations as the lowest integrated water column DSi (Figure 3b, see also Appendix C).

3.1.2. Diatom productivity

Surface $bSiO_2$ production among the three sampling regions ranged from 0.05 – 0.31 µmol Si L^{-1} d^{-1} (Figure 4). For the most part, rates declined with depth; however, the Orphan Knoll site had subsurface maxima at the 20% isolume (~10-20 m) and base of the euphotic zone (i.e. 1% isolume, 20-50 m). The production rates of $bSiO_2$ among the Nuuk profiles were typically higher than Orphan Knoll and Southern Greenland (Figure 4); however, samples incubated in the dark (collected from below the euphotic zone) in Nuuk still had measurable production.

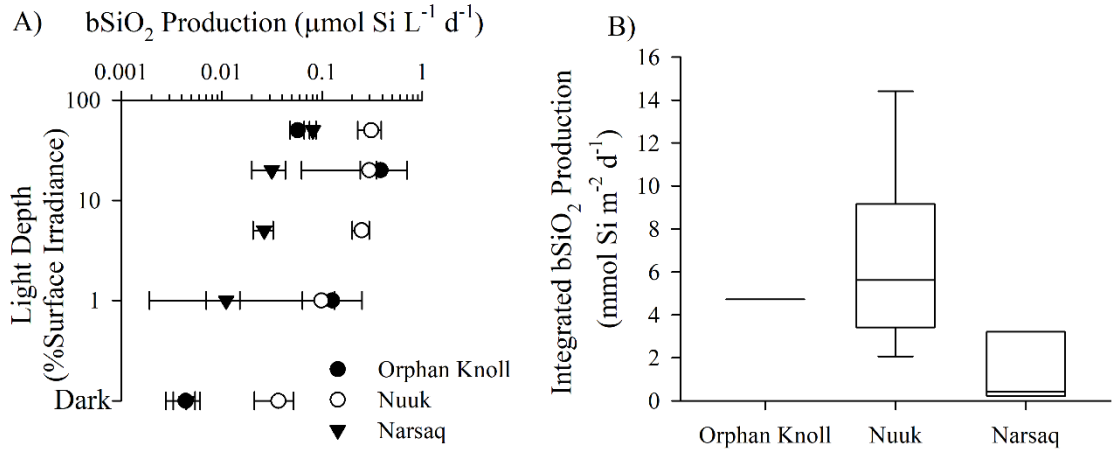

Figure 4: Biogenic silica ($bSiO_2$) production during ICYLAB. A) Averaged (±1SD) gross rates of $bSiO_2$ production (µmol Si L^{-1} d^{-1}) versus relative light depth (i.e. 100% is surface, 1% is base of the euphotic zone) among profiles within Orphan Knoll (filled circles), Nuuk (open circles), and Narsaq (filled triangles). B) Box plots of euphotic-zone integrated $bSiO_2$ production (mmol Si m^{-2} d^{-1}) for profiles in Orphan Knoll (n = 2), Nuuk (n = 9), and Narsaq (n = 6).

3.1.3. Sediment dissolved silicon profiles

Pore water DSi collected from the mega cores and the ROV push cores from the Labrador Sea and coastal Greenland during DY081 expedition range from 49–616 µM (Figure 5). All cores generally show an initial increase in pore water DSi with core depth, indicating

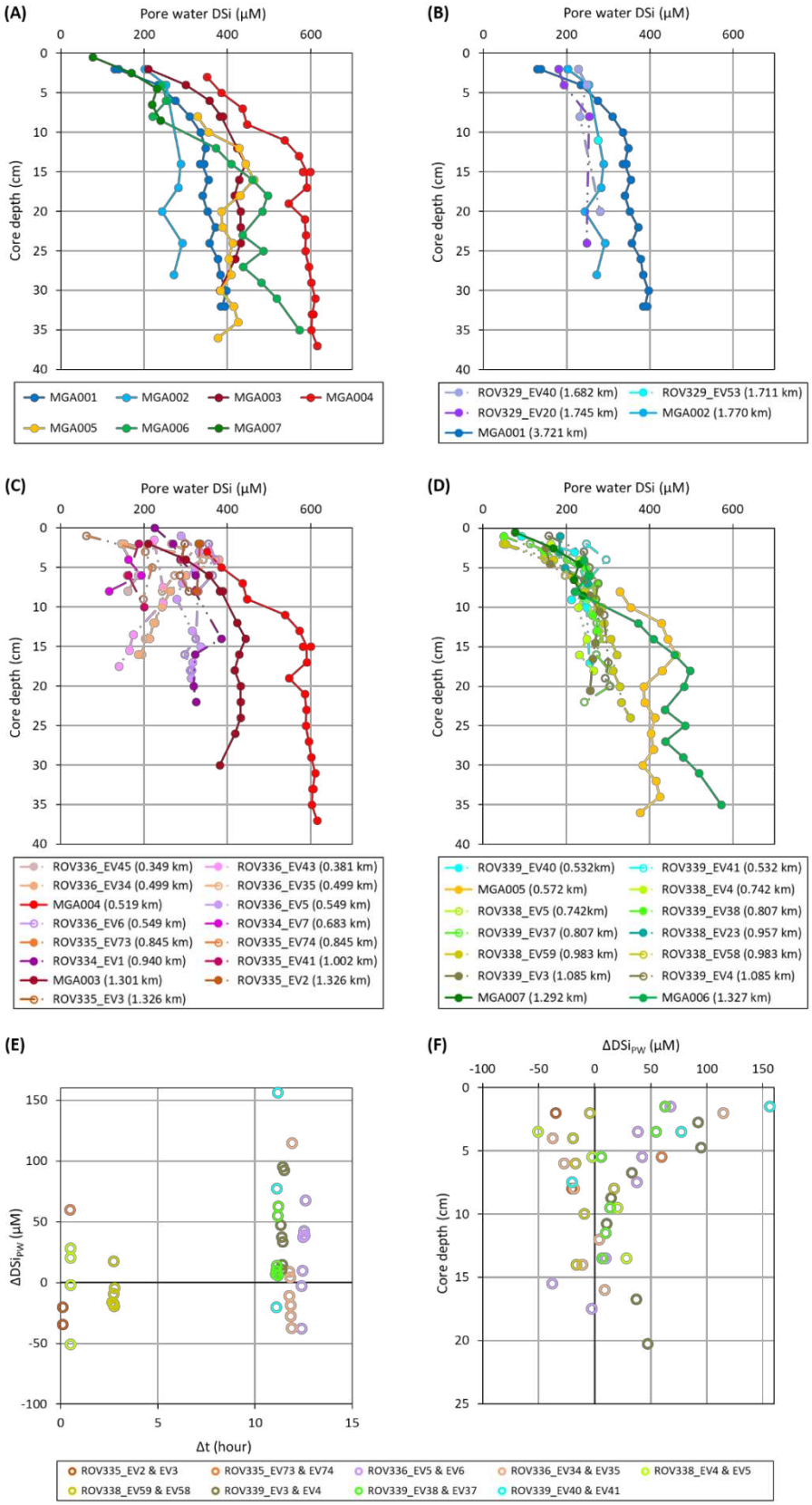

Figure 5: Pore water dissolved silicon concentration (DSi) measurements versus mega core (MGA, solid lines) or ROV push core (dash-dot lines) depths. Results from (a) mega cores, (b) Orphan Knoll cores, (c) cores off Nuuk, and (d) cores off Narsaq and Cape Farewell. Empty circles are results from replicate push cores retrieved at certain sites. Bracketed numbers in plot legends indicate water depths of the sediment cores.

Differences in pore water dissolved silicon concentration between replicate push cores that were sampled at different time periods (ΔDSiPW). ΔDSiPW was calculated by subtracting push core pore water DSi sampled at the latter time period from the corresponding replicate push core pore water DSi sampled at the earlier time period. The calculation was carried out between measurements from the same or nearby (≤ ±1 cm) sediment core depths. (e) ΔDSiPW versus the time difference between the sampling periods of the replicate cores (Δt), (f) ΔDSiPW versus core depth.

346 supply of Si to bottom waters from the sediment via dissolution. At greater depths, the rates
347 of increase of pore water DSi with depth slow down or even reverses (Figure 5).
348 There is good agreement between pore water DSi results (Figure 5) observed in ROV push
349 cores and mega cores from Orphan Knoll and South Greenland (off Narsaq and Cape
350 Farewell). To the best of our knowledge, this is the first formal comparison of pore water
351 DSi profiling using ROV push cores compared to megacorers, and our results provide
352 confidence to the application of this sampling methodology in future studies, especially in
353 settings where the use of a megacorer proves to be challenging (e.g. complex bathymetry,
354 presence of coarse ice-rafted material). In contrast, there is larger variation in pore water
355 DSi (Figure 5) among the sites off Nuuk (Appendix C), which could in part be related to the
356 greater variability in sediment composition (e.g. ice-rafted debris, fossil fragments) and
357 characteristics (e.g. grain size) observed at these sites. More importantly, the highest pore
358 water DSi concentrations are observed (Figure 5) at the shallowest coastal site closest to
359 Nuuk (Appendix C), which is under the influence of meltwater from glacial fjords.
360 Replicate ROV push cores were collected at certain sites to evaluate any consistent
361 change in pore water DSi with time when the sediment cores were left standing onboard at
362 ambient temperature. Results show only minor discrepancies in pore water DSi: up to ±60
363 µM when the sampling was carried out on paired replicate cores within 3 hours of each
364 other (Figure 5); this is likely due to spatial heterogeneity in sediments and pore waters. In
365 contrast, when pore water sampling was carried out on paired replicate cores more than 10
366 hours apart from each other, there are greater discrepancies with higher DSi values
367 measured in the pore water sampled later in time (Figure 5). Our results suggest that pore
368 water in the upper core depths might not reflect original DSi values if the sampling is carried
369 out more than 10 hours after retrieval of the sediment core.
370
371

4. Discussion

Our multi-disciplinary framework allows a nuanced understanding of the whole silica cycle in this climatically critical region, and specifically, the impact of glacial meltwater in shelf seas and into the open ocean. We are able to address questions surrounding the amount of meltwater reaching the ocean, the mechanism by which it does so, and identify mechanisms for how the meltwater is entrained in coastal and boundary currents. For the main context of this study, we can then use this information to understand better the implications of meltwater inputs on macronutrient distributions and biological production, in particular the supply and uptake of DSi. Lastly, we use our palaeoclimate archives to interrogate past changes in meltwater supplies, which are likely to have had a major impact on nutrient cycling.

4.1. Bathymetric features and their role in shelf-water dynamics

The shipboard bathymetric and backscatter data provided a rapid insight into the geomorphology of the study regions. The bathymetry features, resulting from their glacial history, are likely to be an important influence on modern shelf-water dynamics and biogeochemical cycling. The bathymetric grids obtained off the W Greenland coast include the dedicated surveys offshore Nuuk, Narsaq and Cape Farewell, in addition to data collected along the transits (Figure 6). They illustrate a wealth of geomorphological features typical of glaciated margins, such as cross-shelf troughs, iceberg ploughmarks, gully systems, submarine canyons and submarine landslides (Dowdeswell, Canals, Jakobsson, Todd, Dowdeswell et al., 2016). Most notably off Nuuk, the inshore-deepening Gothåb (Nuuk) Trough, previously described by Ryan, Dowdeswell and Hogan (2016), is likely to be important in driving instabilities in localised circulation, influencing the mixing of melt and glacially derived material into the shelf waters. The trough harbours a number of drumlins, elongated features typical of glacial weathering, in addition to intricate patterns of iceberg ploughmarks at the shallow trough mouth (Figure 6). Systems of gullies and submarine canyons can be found at both the Gothåb and Narsaq trough-mouth fans, and along the shelf edge (Figure 6). Some of the canyons are cut up to 350 m into the continental slope, and feature steep to near-vertical walls along their flanks together with scoured channels at their floors. Offshore Narsaq, some of the submarine canyons appear to have evolved as a result of retrogressive failures cutting upslope along gullies (Figure 6).

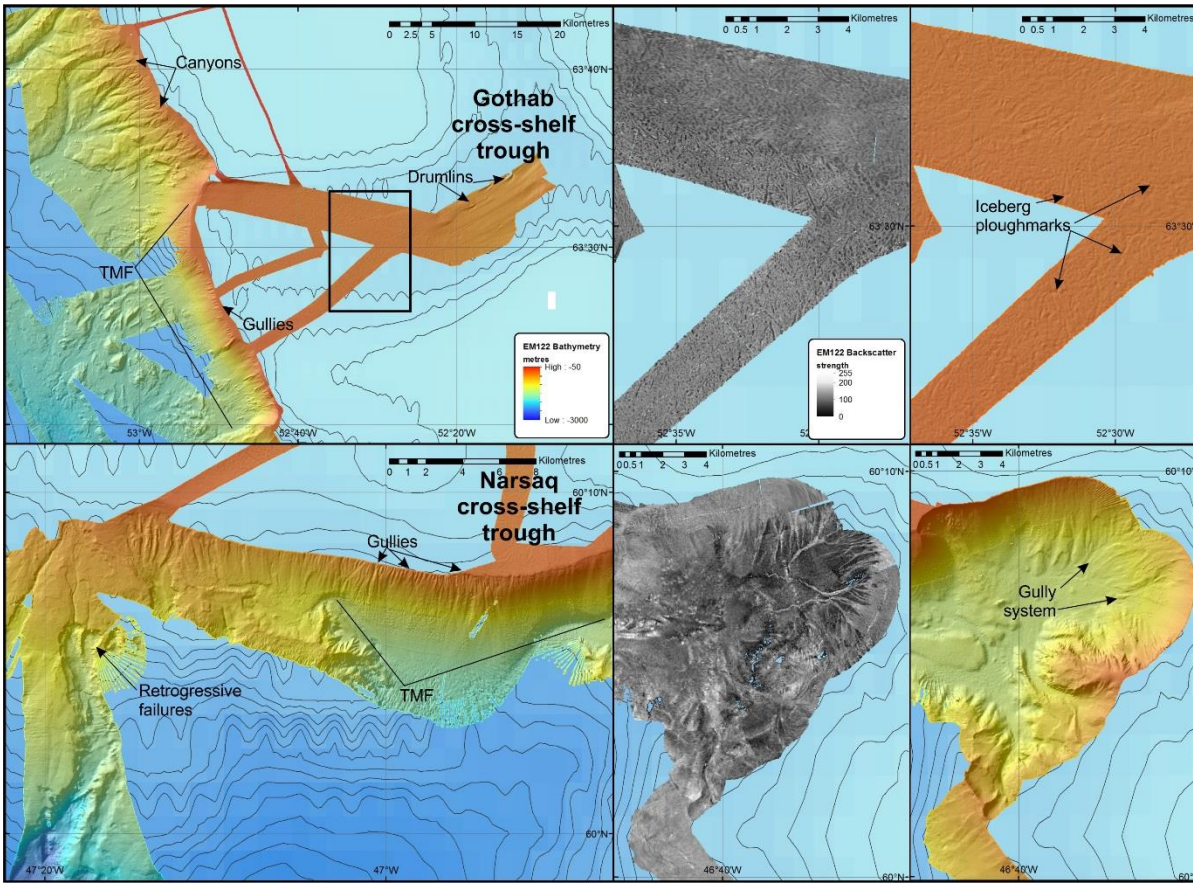

Figure 6: Examples of submarine glacial landforms offshore W Greenland identified in the shipboard multibeam data. Background: bathymetry from ETOPO5 (www.ngdc.noaa.gov/mgg/global/etopo5.HTML), contour interval 100 m. Location of maps indicated on Fig. 1. TMF: trough-mouth fan.

4.2. Physical tracers of glacial meltwater inputs, mixing and advection

We can use the gridded hydrographic and geostrophic velocity fields to constrain the flow of water across the shelf break, focusing on the Gothåb (Nuuk) Trough CTD section (Figure 2b). The subsurface temperature minimum indicates the core of Polar Surface Water, whilst the subsurface temperature maximum is Irminger Water. The Irminger Water is present between 200 m and 700 m over the continental slope, with a core temperature of 4.9°C. There are clear traces of this water mass in the trough also, where warm ($\theta > 4$°C) and saline ($S > 34.7$) water is observed near the bottom at CTD16 and CTD10. The Polar Surface Water core is spread across the whole section at 50-150 m, with minimum temperatures recorded at the station furthest onshore (CTD16).

Geostrophic velocities were calculated by referencing the geostrophic shear to the velocity field measured directly with a Lowered Acoustic Doppler Current Profiler (LADCP). The LADCP velocity field was de-tided, by subtracting the barotropic tide solution obtained from the Oregon State University (OSU) model (Egbert & Erofeeva, 2002). The resultant geostrophic velocity field reveals two surface intensified current cores, one on each side of the trough mouth (Figure 7). The offshore core is associated with a hydrographic front around 15 km west of the shelf break and extends down beyond 400m depth. Its offshore location is consistent with the long-term average position of the West Greenland Current (Myers, Donnelly & Ribergaard, 2009).

The inshore velocity core has a less distinct hydrographic signature and therefore its origin is more uncertain at present. One possibility is that the velocity maximum is the result of topographic steering of the inshore portion of the West Greenland Current by the bathymetric trough. Alternatively, it could represent an eddy of offshore water that has detached from the boundary current. A velocity maximum was also detected in a bathymetric trough inshore of Fylla Bank (near Nuuk) in a numerical model simulation (Myers et al., 2009), but there has been no further study into the nature of this feature to date. Such strong inshore current anomalies have significant consequences for the transport of terrestrially-derived freshwater and nutrients.

In addition to the mean flows, eddies formed from the West Greenland Current transport water from the boundary current to the interior Labrador Sea, where they contribute to the process of Labrador Sea Water formation (Katsman, Spall & Pickart, 2004). Baroclinic instability is thought to be a key formation mechanism, and years of enhanced baroclinicity tend to coincide with high eddy activity (Rykova, Straneo & Bower, 2015), which transfer hydrographic anomalies into the interior. There is significant baroclinicity in both branches of the WGC in our section, implying that eddy generation may be significant. In addition, wind driven Ekman transport is likely to be a key driver in the export of shelf water across the WGC and into the Labrador Sea interior (Schulze & Frajka-Williams, 2018).

Cuny, Rhines, Niiler and Bacon (2002) have suggested that, around this location, the West Greenland Current splits into westward and northward flowing components. However, the location of the splitting, and the partitioning of the water masses involved is not well understood. There are two westward components that flow around the northern perimeter of the Labrador Sea and a northward branch that extends close to the Greenland shelf break

(Cuny et al., 2002). Hydrographic signatures of the West Greenland Current have been reported near Greenland to the north, in the vicinity of Davis Strait and Baffin Bay (Cuny, Rhines & Kwok, 2005; Myers et al., 2009).

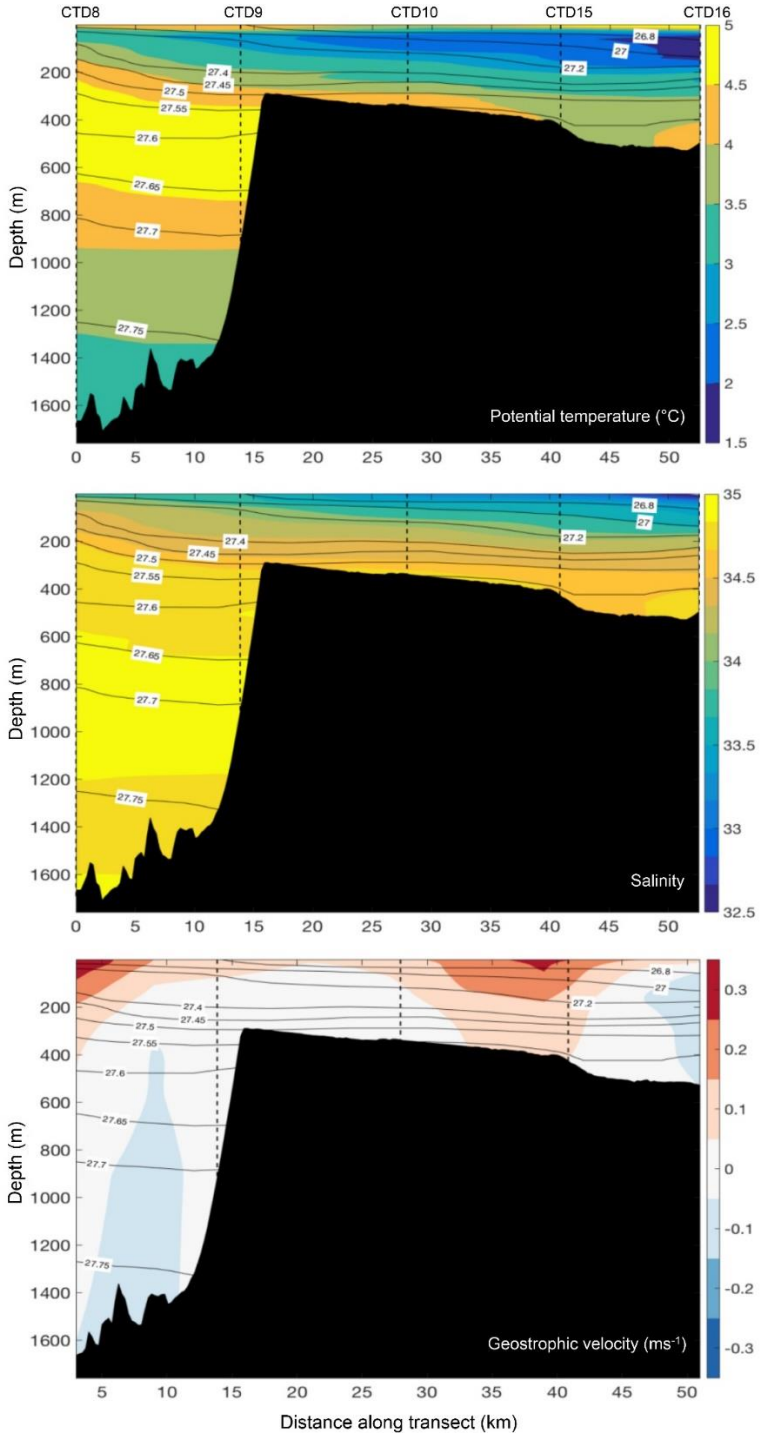

Figure 7: Gridded vertical sections, from top to bottom, of potential temperature (°C), salinity, and geostrophic velocity (m s^{-1}) along Gothåb (Nuuk) Trough. The direction of geostrophic flow is perpendicular to the CTD section (positive northward and negative southward). The black lines with the white boxed labels are isopycnals, which are lines of constant potential density (in kg m^{-3}). The dashed vertical lines indicate the CTD stations, labelled at the top of each panel, from which these vertical sections were derived.

4.3. Chemical tracers of glacial inputs

4.3.1. Chemical tracers of meltwater

Vertical sections of sea ice melt and meteoric percentages based on seawater salinity and $\delta^{18}O$ for the Gothåb (Nuuk) Trough CTD section (Figure 8), reveals a negative offshore gradient in both sea ice melt and meteoric water percentages. Higher freshwater concentrations are found in the trough at all depths, highlighting the potential for glacially-sourced waters to reach the outer shelf and the strong boundary currents.

Freshwater mass balance calculations have, alternatively, been carried out in the High Arctic using salinity and alkalinity endmembers resulting in robust meteoric water percentage reconstructions (e.g. Hendry et al., 2018; Jones, Anderson, Jutterström & Swift, 2008). We compared the two mass balance methods using DY081 data, using both a high meteoric water alkalinity endmember typical of the riverine input to the Arctic Ocean (Jones et al., 2008), and a lower meteoric water alkalinity endmember typical of glacial meltwater (Meire, Søgaard, Mortensen, Meysman, Soetaert et al., 2015). Our comparison indicates that – irrespective of the endmember values chosen - alkalinity-derived values of meteoric water percentages are impacted by subsurface processes that show correlations with nitrite concentrations and temperature (Appendix C). Such non-conservative behaviour likely arises as a result of enhanced alkalinity flux due to water column nitrification, and/or sedimentary denitrification (Fennel, Wilkin, Previdi & Najjar, 2008; Wolf-Gladrow, Zeebe, Klaas, Körtzinger & Dickson, 2007).

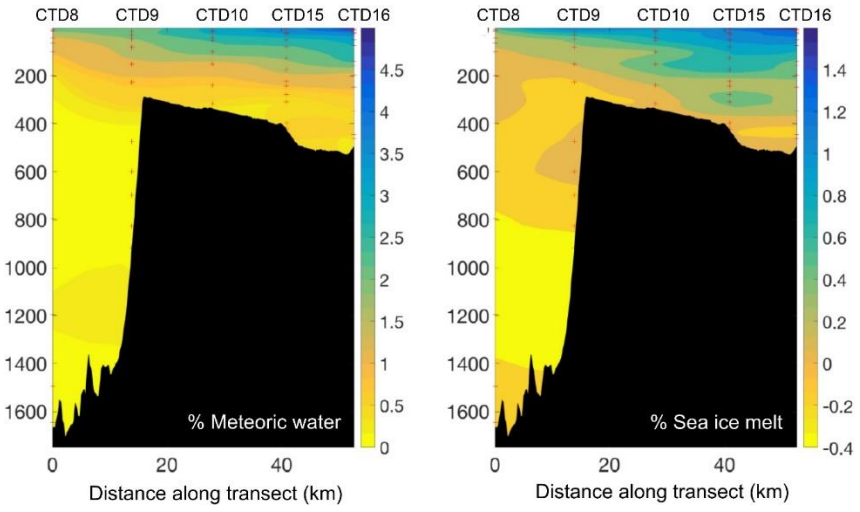

Figure 8: Vertical sections of meteoric water and sea ice melt percentages along Gothåb (Nuuk) Trough. The black area is the bathymetry of the section, as measured by the ship multibeam. Red pluses indicate the bottle sampling locations, with the CTD stations annotated above.

474

475

476 *4.3.2. Geochemical tracers of particulate flux*

477 Radium (Ra) is produced continuously from lithogenic material by the decay of thorium
478 (Th) and thus displays elevated concentrations near any sediment-water interface. Short-
479 lived Ra activities did not show a clear relationship with salinity (Figure 9), but did exhibit
480 informative regional variability. The relatively low activities around Cape Farewell indicate a
481 lack of recent lithogenic input upstream of this region (along the eastern coast of
482 Greenland). From Cape Farewell $^{224}Ra_{XS}$ increases westwards to ~51° W, consistent with
483 increasing cumulative sedimentary inputs into the Greenland coastal current (Figure 9C). As

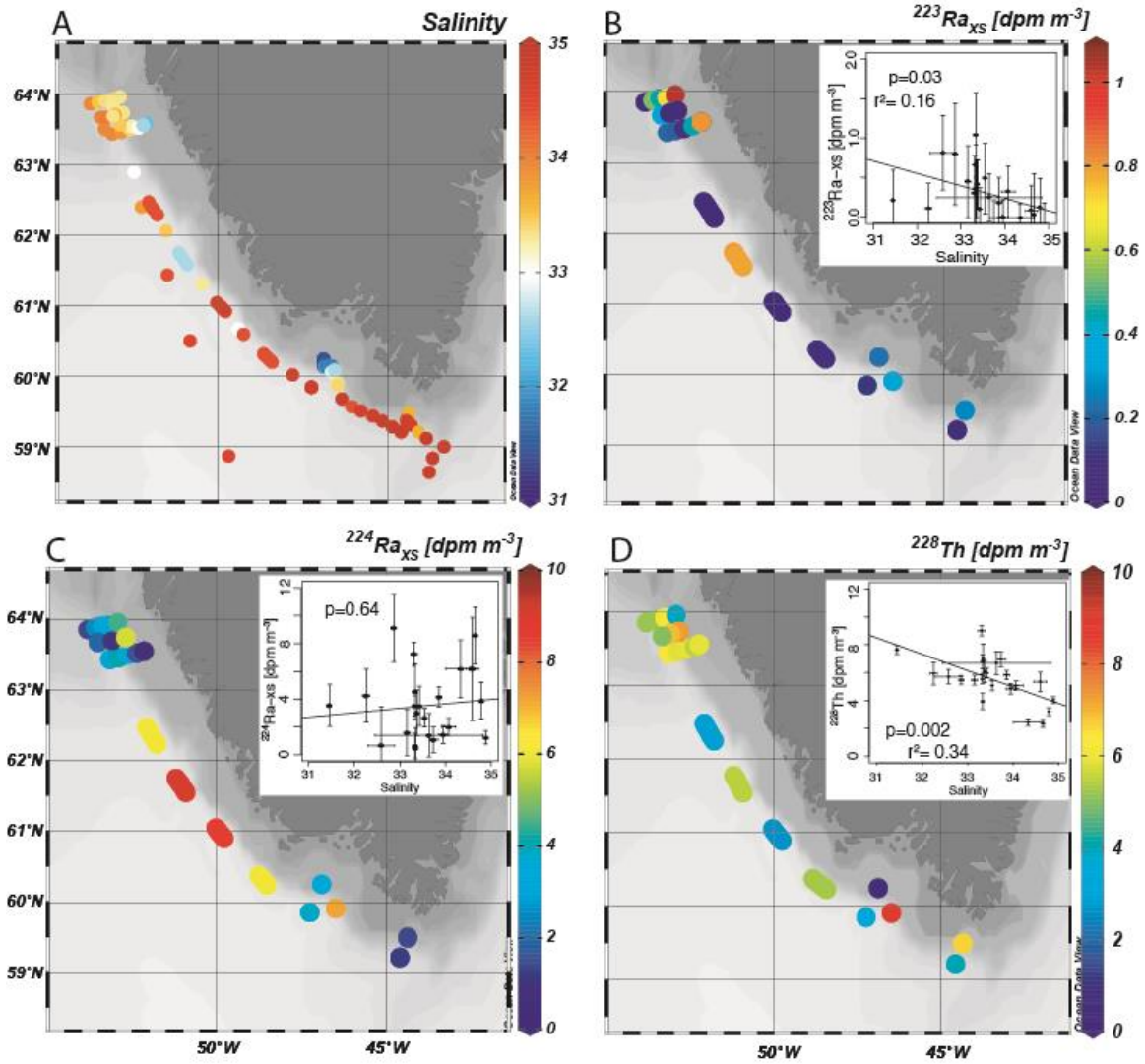

Figure 9: Spatial distribution of salinity (A), $^{223}Ra_{XS}$ (B) $^{224}Ra_{XS}$ (C) and ^{228}Th (D) from towfish samples taken at 2-5 m depth. Elongated symbols show underway samples which took ~1h to collect. For B-D, inset plots show the same isotope versus salinity in surface waters. Vertical error bars denote ±1 standard error for activities, and horizontal error bars show the standard deviation of salinity measurements taken each minute during the ~1 h sampling interval.

CTD profiles show that the shallow surface mixed layer sampled by our towfish extended to only 10-20 m, the most likely sources for $^{224}Ra_{XS}$ are glacial meltwater, very shallow sediments within fjords, or resuspended shelf sediments by storm-driven mixing. This signal then decreases towards Nuuk, which will reflect both dilution due to mixing and decay of the short-lived isotope (half-life 3.66 d), and also suggests minimal further lithogenic input into the surface mixed layer. The difference in activity from ~ 9 dpm m^{-3} at ~51° W to < 4.5 dpm m^{-3} at the Nuuk sampling stations suggests a decay time of one half-life between these sampling regions, a distance of 300-400 km, although dilution or additional inputs would also affect the measured activity and cannot be fully quantified at present. However, the maximum $^{224}Ra_{XS}$ activities of 8-9 dpm m^{-3} above deep water off the shelf break demonstrate that this lithogenic signal is persistent, with the potential to rapidly transport other glacial and sedimentary-derived compounds far offshore.

Although this spatial pattern is not clear in the longer-lived $^{223}Ra_{XS}$ (Figure 9B), the lower overall activity of this isotope - as well as lower detection efficiency - lead to lower signal to noise ratios. It is also likely that regional lithologies may lead to different input patterns due to differing distribution of the ^{227}Ac and ^{228}Th parents.

Our analysis also quantifies ^{228}Th, the parent of ^{224}Ra. Due to its lithogenic origin and higher particle reactivity, trends in ^{228}Th may be more closely associated with particulate phases than Ra, especially in our unfiltered samples. Samples collected on fibre are generally assumed to retain the majority of both particulate and dissolved Th, although in coastal waters this approach may underestimate total ^{228}Th where particles can be flushed through the sample, and the activities presented here also include supported activity from ^{228}Ra (the parent of ^{228}Th) within the water column. Nevertheless, our ^{228}Th data (Figure 9D) shows a statistically significant correlation with salinity. We therefore suggest that contrasting patterns in the $^{224}Ra_{XS}$ daughter may be attributed to additional inputs from fjord or shallow shelf sediments, as these inputs are more significant for dissolved species. Additional samples from inner fjord locations and depths below the mixed layer will enable us to differentiate between inputs from marine and glacial sediments.

4.4. Diatom productivity in glacially-influenced shelf seas

Despite the low nutrient concentrations, $bSiO_2$ production rates were significant in the meltwater influenced waters off the shelf and slope. Similar surface DSi concentrations are

observed in the open-ocean gyres (e.g. North Pacific, Brzezinski, Krause, Church, Karl, Li et al. (2011); North Atlantic, Krause, Nelson and Lomas (2010)) and typically do not support high rates of diatom productivity. Spring-season $bSiO_2$ production rates in Svalbard and the Barents Sea (Krause, Duarte, Marquez, Assmy, Fernández-Méndez et al., 2018) and at the MarineBasis Nuuk station in Godthaabsfjord (Krause, Schulz, Rowe, Dobbins, Winding et al., In review) were routinely lower than those quantified at Orphan Knoll or Nuuk. The active production below the euphotic zone suggests either recently exported diatoms (e.g. from surface waters within 1-2 days) or the presence of siliceous and active Rhizaria (Biard, Krause, Stukel & Ohman, 2018; Biard, Stemmann, Picheral, Mayot, Vandromme et al., 2016). Integrated $bSiO_2$ production rates in the euphotic zone ranged two orders of magnitude, 0.13 – 14.4 mmol Si m^{-2} d^{-1}. Four of the six stations off Southern Greenland had integrated rates <1 mmol Si m^{-2} d^{-1}, similar to mid-ocean gyres (Brzezinski et al., 2011), whereas all other profiles during the cruise exceeded 2 mmol Si m^{-2} d^{-1}. These rates are on the lower end for the Southern Ocean (1-93 mmol Si m^{-2} d^{-1}, Nelson, Treguer, Brzezinski, Leynaert and Queguiner (1995)) but are similar to Svalbard and the Barents Sea during spring (0.3–1.5 mmol Si m^{-2} d^{-1}, Krause et al. 2018). Overall, diatom $bSiO_2$ production consumed 4% (median) – 10% (average) of the euphotic zone DSi inventory daily. These data are the first such reports for this region of the Labrador Sea and Greenland, and demonstrate a surprisingly active diatom assemblage despite low nutrients, temperature, and biomass.

4.5. Influence of glacial meltwaters in the open ocean: Si cycling as a case study

Although glacial meltwaters exhibit elevated concentrations of some dissolved nutrients and reactive phases (e.g. Hawkings et al., 2017), glacial fjords – the conduits between the source of these nutrients and the open ocean – are characterised by complex physical, chemical and biological processes and are highly variable in space and time (Hopwood, Carroll, Browning, Meire, Mortensen et al., 2018). Despite the highly heterogeneous nature of these environments, we can use the findings from DY081 to shed more light on the key common processes that characterise the transfer of nutrients across the land-ocean interface, which will likely vary in rates and importance between different glaciated regions.

In many high-latitude regions, upwelled waters are thought to dominate the supply of nutrients to the euphotic zone supporting most of the primary production. For example, off the West Antarctic Peninsula (WAP), biological “hotspots” were thought to be fed by

548 upwelling Circumpolar Deep Water (CDW) being channelled onto the shelf via glacially
549 carved canyons (Schofield, Ducklow, Bernard, Doney, Patterson-Fraser et al., 2013).
550 However, there is increasing evidence that CDW is heavily modified as it transits onto the
551 shelf likely due to a flux of silica and iron from shallow marine sediments (Henley et al.,
552 2018; Sherrell et al., 2018). However, even in these relatively nutrient-rich environments,
553 there is still some important direct input from glacial meltwaters (e.g. Annett, Skiba, Henley,
554 Venables, Meredith et al., 2015) due to the release of reactive phases and promotion of
555 biological mediation of nutrient cycling through the formation of organic matter and
556 biogenic minerals.
557 Despite different boundary conditions compared to the WAP, similar processes are likely
558 to be happening in glaciated regions of SW Greenland. For example, elevated DSi (>20 μM)
559 in Greenlandic fjords measured in surface waters (Hawkings et al., 2017) cannot simply be
560 explained by mixing between the freshwater and marine end-members: these
561 concentrations are higher than the freshwater endmember, and there are no seawater
562 masses with sufficiently high DSi concentrations in the top 100m to supply this flux (Figure
563 3, see also Appendix C). The fjord water must be modified – in an analogous way to the WAP
564 – likely by particle-water interactions, including the release of DSi from reactive phases
565 derived from glacial weathering products, or biogenic silica (Hawkings et al., 2018; Hawkings
566 et al., 2017; Meire et al., 2016). This modification may be active in the water column, as well
567 as at the sediment-water interface, in the fjords as well as in the shallow water shelf-
568 sediments (Figure 5).
569 However, despite this enrichment within the fjord, the low-salinity waters reaching the
570 coastal ocean are low in DSi as a result of uptake mechanisms that are active as the fjordic
571 waters reach the shelf; our forthcoming studies of uptake kinetics and algal physiology from
572 within the fjords themselves will elucidate whether biological uptake is playing a key role in
573 Si cycling in these regions. Although there is apparently a limited supply of DSi exported
574 from fjords, there appears to be active cycling of silica by diatoms in coastal waters. Our
575 findings show the potential for meteoric waters, and glacially-derived particles, to be
576 exported as far as the coastal and boundary currents, and into the open ocean, where
577 further processing could act to release bioavailable elements. Whilst some of these
578 exported particles may dissolve within the water column during sinking, some will reach the
579 sediment-water interface. Pore water DSi can be used to evaluate the chemical changes of

580 the sediments post-deposition such as the dissolution of this reactive glacial material in
581 addition to dissolution of biogenic silica remains of diatoms and sponges, secondary or
582 'reverse' weathering, and the recycling of DSi back to the bottom waters (Rahman, Aller &
583 Cochran, 2017). The high, but variable, DSi concentrations found in the pore waters at our
584 coastal study sites point towards high rates of benthic regeneration fluxes. Calculated
585 sedimentary diffusive fluxes off SW Greenland, using the approach of Ragueneau, Gallinari,
586 Corrin, Grandel, Hall et al. (2001), range from 0.1-0.3 mmol Si m^{-2} d^{-1}, and are at least 10% of
587 the diatom production rates. Our findings suggest that the total DSi flux across the
588 sediment-water interface, including from advective processes, could rival the magnitude of
589 water column biogenic silica production rates. The high uptake rates of diatoms, together
590 with this rapid recirculation of DSi across the sediment-water interface, points towards a
591 silica cycle maintained by strong pelagic-benthic coupling.
592
593 **4.5. Approaches to reconstructing glacial meltwater inputs through time**
594 Glacial meltwaters are enriched in both dissolved and particulate nutrients, including
595 silicon, and our new data highlight that these meltwaters extend across the shelf into
596 boundary currents. In the context of the marine silicon cycle, our data show that, whilst DSi
597 reaching the shelf waters from the glacial fjords may be low, diatom activity is surprisingly
598 high. DSi must be reaching the surface, potentially by mixing with modified shelf waters. Our
599 Ra isotopic data (section 4.3.2.) reveal that there is input of glacial particles into these shelf
600 waters, potentially via sediment reworking, which may contribute bioavailable silicon via
601 dissolution both in the water column and at the sediment-water interface. This system is
602 likely to be sensitive to glacial inputs, and so quantifying changes in meltwater fluxes
603 through time - using a variety of climate archives - is going to be key to understanding shelf
604 and slope productivity during past episodes of climatic change.
605
606 *4.5.1. Fossil deep-sea corals*
607 The geochemistry of fossil skeletons of deep-sea corals has the potential to record
608 aspect of past environmental conditions (Chen, Robinson, Beasley, Claxton, Andersen et al.,
609 2016; Robinson, Adkins, Frank, Gagnon, Prouty et al., 2014). In particular, water masses
610 distribution and food supply are thought to be important for deep-sea coral populations off
611 the West Greenland margin. Given their environmental sensitivity, cold-water coral

distributions are likely to susceptible to changes in water mass properties and primary production caused by meltwater inputs. In 2017, the first living samples of the cold-water scleractinian coral*, Lophelia pertusa*, were collected from approximately 60° 22'N off the Greenland within a layer of relatively warm, modified Atlantic Water (Kenchington, Yashayaev, Tendal & Jørgensbye, 2017).

We have now been able to make in situ observations of cold water corals off Greenland, as well as showing that corals have been present on the Greenland Margin for at least 10,000 years (Figure 10). These first populations likely appeared with melting of the large ice fields of the last glacial period. Supporting prior research, we also found that scleractinian corals have been present further south on Orphan Knoll for at least 130,000 years (Figure 10; Cao, Fairbanks, Mortlock & Risk, 2007; Hillaire-Marcel, Maccali, Ménabréaz, Ghaleb, Blénet et al., 2017). In both locations our suite of dates show that the populations have not been stable. This observation implies shifts in environmental pressures over these timescales, likely driven by a shift in balance between warmer Atlantic waters and cold meltwater-rich polar waters.

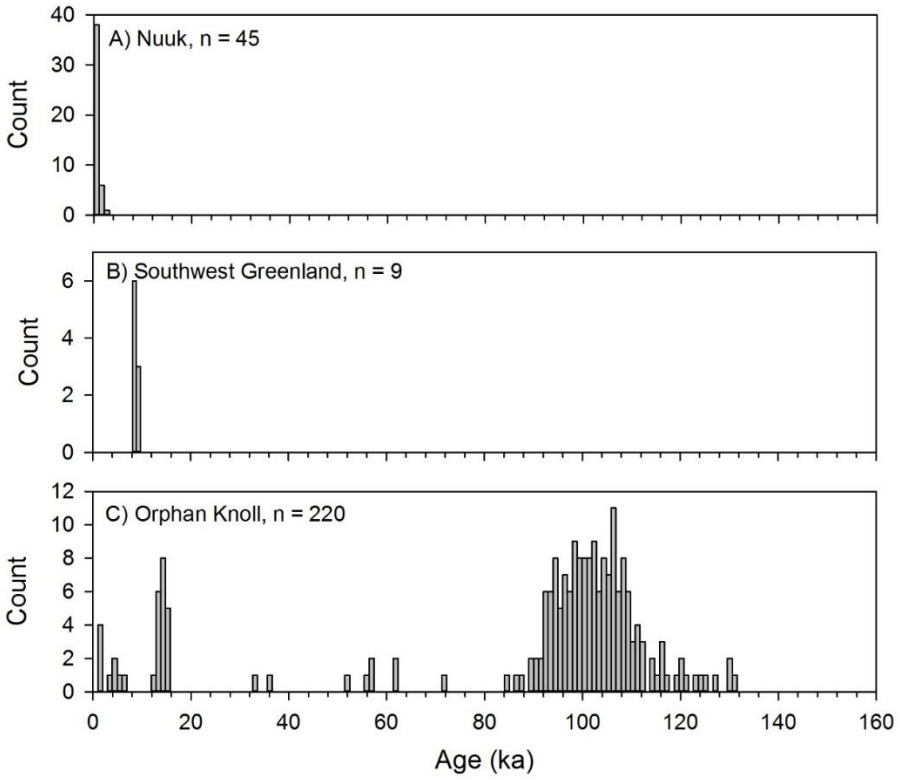

Figure 10: Uranium-thorium age data for fossil corals collected during DY081.

628 *4.5.2. Marine sediments and past glacial meltwater inputs*

629 During the last ice age, catastrophic iceberg discharge events episodically flooded the
630 subpolar North Atlantic with meltwater (Heinrich, 1988). Evidence suggests that these
631 "Heinrich events" (Broecker, Bond, Klas, Clark & McManus, 1992), were related to, and may
632 have acted as the trigger for (Broecker, 2003; Clark, Pisias, Stocker & Weaver, 2002),
633 dramatic changes in ocean circulation (McManus, Francois, Gherardi, Keigwin & Brown-
634 Leger, 2004) and heat distribution that were felt globally (e.g. Wang, Cheng, Edwards, An,
635 Wu et al., 2001). In addition to global impacts, changes in ice sheet dynamics and meltwater
636 inputs would also have had considerable impacts on more regional biogeochemical cycling.
637 While previous work has identified the existence of eight such events over the last 70 ka
638 (Andrews, Jennings, Kerwin, Kirby, Manley et al., 1995; Bond, Heinrich, Broecker, Labeyrie,
639 McManus et al., 1992; Bond & Lotti, 1995; Rashid, Hesse & Piper, 2003; Stoner, Channell &
640 Hillaire-Marcel, 1996), questions remain about the origin(s) of these events, their trigger(s)
641 and the nature of their primary signatures across the North Atlantic (Andrews & Voelker,
642 2018). Gravity cores collected at Orphan Knoll (DY081-GVY002 & GVY002), Southwest
643 Greenland (DY081-GVY003) and Cape Farewell (DY081-GVY004 & GVY 005) represent new
644 opportunities to constrain the timing, geometry and character of iceberg discharge and
645 glacial meltwater release in the paleo record.

646 Existing work on marine sediment cores from the high latitude North Atlantic has
647 employed a variety of proxies to identify pulses of meltwater delivery and associated ice
648 rafted debris delivery. Previously applied proxies include $^{230}Th_{xs,0}$ (to assess changes in
649 sedimentary fluxes (McManus, Anderson, Broecker, Fleisher & Higgins, 1998)), counts of IRD
650 and foraminifera (to identify the relative abundance of terrestrially-derived debris and
651 foraminifera (Heinrich, 1988)), foraminifera census (to determine the relative abundance of
652 cold-dwelling planktonic species such as *N. pachyderma s.* (Ruddiman, Sancetta &
653 McIntryre, 1977)), $\delta^{18}O$ of *N. pachyderma s.* (to quantify the cooling and/or freshening of
654 surface waters (Bond, Broecker, Johnsen, McManus, Labeyrie et al., 1993)), magnetic
655 susceptibility (to identify detrital sediment (Grousset, Labeyrie, Sinko, Cremer, Bond et al.,
656 1993)), x-ray diffraction (XRD) (to assess changes in the abundance of quartz and plagioclase
657 feldspar (Moros, Kuijpers, Snowball, Lassen, Bäckström et al., 2002; Moros, McManus,
658 Rasmussen, Kuijpers, Dokken et al., 2004)), and X-ray fluorescence (XRF) (to identify changes
659 in sedimentary elemental ratios (Hodell, Channell, Curtis, Romero & Röhl, 2008)).

Unfortunately, the comparison of sediment core records has been limited by difficulties in establishing tightly constrained chronologies. This has impeded analysis of the triggers of events and the range of their influence (Andrews & Voelker, 2018). While previous work has utilized one or more of the proxy approaches identified above, complete assessment of the proxies described above, in a single core, would greatly assist in interpreting the paleoceanographic record. In addition, despite the widespread inference that icebergs originated from the Laurentide ice sheet during these events (Bond & Lotti, 1995; Broecker, 2003; Hodell et al., 2008; McManus et al., 1998), relatively fewer detailed studies have examined their imprint and consequences in the proximal Labrador Sea (Andrews & Voelker, 2018).

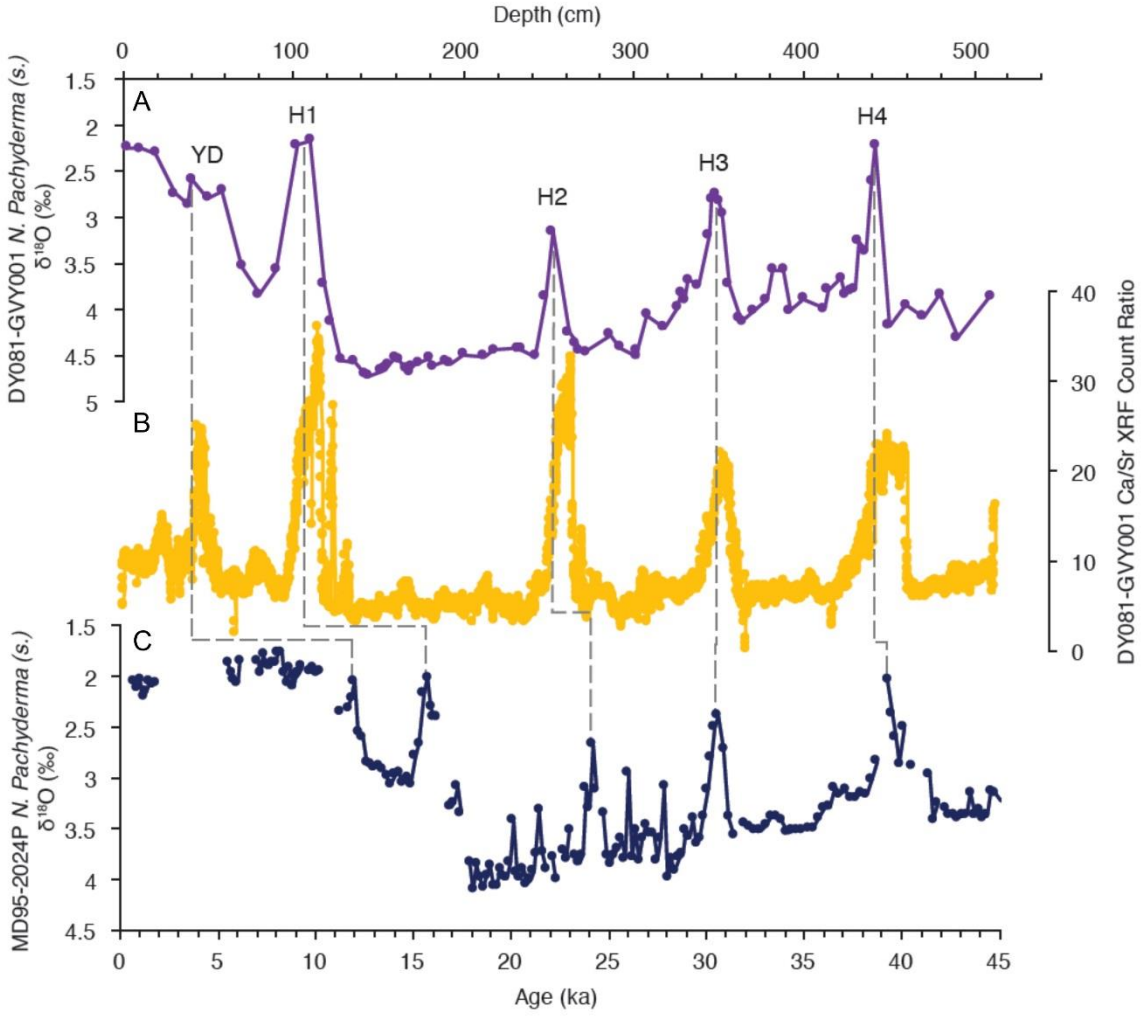

Figure 11: Proxies for North Atlantic Heinrich Events. a) N. Pachyderma (s.) $\delta^{18}O$ from DY081-GVY001 (purple). b) Ca/Sr XRF count ratio from DY081-GVY001 (yellow). c) N. Pachyderma (s.) $\delta^{18}O$ (Hillaire-Marcel & Bilodeau, 2000) on the age model of Lynch-Stieglitz, Schmidt, Henry, Curry, Skinner et al. (2014) (navy blue). Vertical grey dashes suggest age-depth assignments for DY081-GVY001.

Our goal in analysing the new DY081 cores is to use a wide range of proxies to address temporal relationships and the spatial signatures of Heinrich events. Our findings show that GVY001 (Orphan Knoll) represents a record of continuous sedimentation from 40-50 ka to present and likely captures the Younger Dryas and Heinrich events 1-4 (Figure 11). In GVY001 Heinrich event signatures have been identified in records of IRD counts, the $\delta^{18}O$ of planktonic foraminifera, XRD and XRF scans. These results confirm the utility of using the suite of proxies in DY081 cores to tie together previously incomparable records from sediment cores in which disparate proxies have been applied, to reconstruct meltwater inputs in the region back through time.

5. Synthesis and Outlook

Coastal and shelf sea biogeochemical research in the polar regions requires high-resolution spatial and temporal datasets, due to the inherent heterogeneous nature of the high-latitude margin settings. Whilst obtaining the necessary temporal resolution is challenging, especially in the absence of expensive long-term monitoring programs, it is possible to combine traditional physical and biogeochemical measurements with novel isotopic and observational methods that integrate signals over a variety of timescales (days to thousands of years). Stable and radiometric isotope geochemistry also allows the identification of common processes within this highly-variable system, which are active over given timescales. All of these approaches can be combined with palaeoceanographic techniques to obtain a reliable baseline for pre-industrial conditions, and also look for analogues of future change from the past.

In the context of the marine silica cycle, our findings from DY081 are able to show that:

- There are strong mean flows that are conducive to eddy generation, which will likely transport freshwater from the margin into the boundary currents that supply the Labrador Sea;
- Oxygen isotopes robustly trace meteoric water composition adjacent to Greenland, with near-surface concentrations of 5% over the shelf reflecting significant glacial discharge;
- Ra isotopes indicate additions of glacial meltwater and sedimentary particulates are spatially heterogeneous and rapidly transported;

- Low macronutrient concentrations (e.g. DSi) are found in coastal waters influenced by glacial melt;
- Diatoms are surprisingly active given the low nutrient availability and low temperature (i.e. consuming 5-10% of euphotic zone Si daily);
- There is a strong benthic flux of DSi from sediments;
- Fossil corals can be used to track changes in benthic ecosystems through time, likely influenced by water mass distribution;
- Sediment cores recovered of sufficient length and resolution to reconstruct meltwater inputs at least back to 45 ka (i.e. Heinrich events 0-4).

Acknowledgments

The authors would like to thank the Captain and crew of the RRS *Discovery*, the National Marine Facility technicians, David Turner, and project manager, Daniel Comben, National Oceanography Centre Southampton (NOCS). Many thanks to Sinhue Torres-Valdes and Christopher D. Coath for assistance in the laboratory, and the Marine Geoscience group at NOCS for providing the core-splitter. Funding for DY081 was from the European Research Council (ERC Starting Grant 678371 ICY-LAB). The contributions of AWJ, GGC, and JFM were supported in part by the US-NSF.

722

723 Table 1: End-member values used in the mass balance calculations.

	Irminger	Meteoric	Sea ice
Salinity	34.88	0	3
$\delta^{18}O$ (‰)	+0.34	c. –21	Surface values +2.1

724
725

APPENDIX A: Oceanographic setting

The strong West Greenland Current (WGC) brings cold Arctic Water (AW) around the southern tip of Greenland and northwards into the Labrador Sea (Yang et al., 2016). The Irminger Current (IC) brings in warmer North Atlantic Water (NAW) from the North Atlantic into the Labrador Sea – this water is ultimately derived from the Gulf Stream. The typical water column structure near coastal Western Greenland is stratified by salinity, comprising cold, surface water (found shallower than approximately 100 m) that consists of AW and additional meltwater, overlying a strong thermocline; NAW (temperature > 3˚C, salinity < 34.5) is found below the thermocline, with the water temperature peaking at a depth of approximately 400m, most likely representing the core of Irminger Water inflow (McCartney and Talley, 1982).

At approximately 64 °N, the latitude of Nuuk, the WGC bifurcates into the Labrador Current (LC), and a proportion is diverted into the interior of the Labrador Sea, where deep water formation occurs by winter-time convection driven by oceanic heat loss (McCartney, 1992). The newly formed Labrador Sea Water (LSW) enters the North Atlantic as the Deep Western Boundary Current, to form the upper layers of North Atlantic Deep Water (NADW), which subsequently become the intermediate layers of the North Atlantic meridional overturning circulation. By the time the boundary current reaches Orphan Knoll (Figure 2a), sub-thermocline warm, saline waters are underlain by the LSW and overflow waters (likely Gibbs Fracture Zone Water and Demark Strait Overflow Water) (Yang et al., 2016).

APPENDIX B: Details of methodologies

Full details of on-board methodology and approach can be found in the DY081 cruise report (Hendry, 2017), but are summarised briefly here.

B.1. Water column sampling and on-board processing: glacial meltwater inputs, nutrients, and phytoplankton

Water column samples were collected using Niskin bottles attached to the CTD rosette (10L volume) and the Remotely Operated Vehicle (ROV) *Isis* (4 L volume), and via a trace-metal clean towfish.

759 Duplicate samples for inorganic macronutrients were filtered using either an Acropak
760 or in-line polycarbonate filter (0.2 μm) into acid-cleaned and rinsed high density
761 polyethylene (HDPE) bottles and frozen immediately at -20˚C. Clean handling techniques
762 were adopted and only Semperguard vinyl non-powdered gloves were used for the sample
763 handling. Samples for biogenic/amorphous silica were filtered through 25mm 0.6 μm
764 polycarbonate filters, dried and stored for analysis back on land.
765 Samples were also collected for water oxygen isotope composition ($\delta^{18}O$) and
766 carbonate chemistry parameters (pH, alkalinity), which are used for investigating freshwater
767 input in high-latitude regions (Hendry et al., 2018; Meredith et al., 2008; Thomas et al.,
768 2011). For $\delta^{18}O$, an unfiltered water sample was sealed tightly in a (rinsed) 60 mL HDPE
769 plastic bottle and stored in a cool, dark storage location. For carbonate chemistry, a 250 mL
770 borosilicate glass bottle was rinsed twice with seawater from the Niskin before being filled
771 using a PVC tube and allowed to overflow one volume; a glass stopper was placed in the
772 bottle neck to displace excess seawater then 2.5 mL of seawater was pipetted off to allow a
773 1% headspace. The sample was poisoned with 50 μL saturated mercuric chloride solution
774 and sealed, homogenised and stored in a cool, dark storage location.
775 Phytoplankton pigments were analysed on board, and compared to sensor-derived
776 fluorescence data, to assess algal standing stocks in relation to meltwater input. Seawater
777 was filtered using GF/F filters and then frozen at -20 ˚C until extraction. A trichromatic
778 method (Mackereth et al., 1978) was used to determine chlorophyll (Chl) a, b, and c
779 spectrophotometrically in the near surface seawater samples. Chlorophyll extraction was
780 carried out using aqueous acetone buffered with magnesium carbonate, for 24 hours in the
781 dark at 4˚C. The samples were then centrifuged and analysed at 750 nm (to correct for
782 turbidity), 664 nm, 647 nm, and 630 nm on a V-1200 Vis spectrophotometer. Absorbance
783 values were then used in equations 1 to 3 to calculate the concentration of Chl *a, b*, and *c*
784 per volume of filtered sample (Eq. 4).
785 Chl *a* (mg/L) = 11.85*(OD664) – 1.54*(OD647) – 0.08*(OD630) (1)
786 Chl *b* (mg/L) = 21.03*(OD647) – 5.43*(OD664) – 2.66*(OD630) (2)
787 Chl *c* (mg/L) = 24.52*(OD630) – 7.60*(OD647) – 1.67*(OD664) (3)
788 Chl *x*, mg/m^3 = (Chl *x*) * extract volume, L/ Volume of sample, m^3 (4)
789

B.2. Additional laboratory techniques

Seawater oxygen isotope ($\delta^{18}O$) measurements were made using the CO_2 equilibration method with an Isoprime 100 mass spectrometer plus Aquaprep device at the British Geological Survey (Keyworth). 200µl samples of water were loaded into exetainers (3.7ml Labco Ltd.) and placed in the heated sample tray at 40°C. The exetainers were then evacuated to remove atmosphere, then flushed with CO_2 and left to equilibrate for between 12 (first sample) - 37 (last sample) hours. Each individual gas sample was then admitted to the cryogenic water trap where any water vapour was removed. The dry sample gas was then expanded into the dual inlet where it was measured on the transducer before being expanded in the dual inlet bellows. Ionvantage software balanced the reference bellows relative to its volume. The sample and reference CO_2 gases entered alternatively into the Isoprime100 through the dual changeover valve for isotope ratio measurement. In each run two laboratory standards (CA-HI and CA-LO) plus up to two secondary standards were analysed in triplicate. The value of these laboratory standards has been accurately determined by comparison with international calibration and reference materials (VSMOW2, SLAP2 and GISP) and so the $^{18}O/^{16}O$ ratios (versus VSMOW2) of the unknown samples can be calculated and are expressed in delta units, $\delta^{18}O$ (‰, parts per mille). Isotope measurements used internal standards calibrated against the international standards VSMOW2 and VSLAP2. Errors are typically +/– 0.05‰ for $\delta^{18}O$.

Carbonate analysis was carried out at GEOMAR, Germany. For Total Dissolved Inorganic Carbon (TDIC), carbonate species were converted to CO_2 by addition of phosphoric acid (10% in 0.7 M NaCl), this generated CO_2 is then carried into the measurement cell using N_2 and analysed by coulometric titration using a VINDTA 3C (Marianda, Germany) connected to a 5011 coulometer (UIC, USA). For Total Alkalinity (TA) samples are titrated with 0.1 M HCl (prepared in 0.7 M NaCl) in 150 µL increments until the carbonic acid equivalence point is reached. The titration is monitored with the VINDTA 3C in a closed cell titration (Dickson et al., 2007). Measurements were calibrated using certified reference material from Prof. Dickson, Scripps. The temperature, salinity, and nutrient concentrations of the samples at time of sampling are then combined with the TDIC and TA measurements to calculate CO_2 system parameters (pH and pCO_2).

Samples for inorganic nutrients were all analysed at the Plymouth Marine Laboratory using the latest GO-SHIP (Hydes et al., 2010) recommended defrosting technique of heating

in a warm water bath for 45 minutes from frozen and then equilibrating to room temperature for another 30 minutes before analysis. The analysis was carried out using a SEAL analytical AAIII segmented flow colorimetric auto-analyser using classical analytical techniques for nitrate, nitrite, silicic acid (or DSi) and phosphate, as described in Woodward and Rees (2001). Clean sampling and handling techniques were employed during the defrosting, sampling and manipulations within the laboratory, and where possible carried out according to the International GO-SHIP nutrient manual recommendations of Hydes et al. (2010). Seawater nutrient reference materials (KANSO Ltd. Japan) were also analysed to check analyser performance and to guarantee the quality control of the final reported data. The typical uncertainty of the analytical results were between 2-3%, and the limits of detection for nitrate and phosphate were 0.02 µM, 0.01 µM for nitrite, and silicic acid did not ever approach the limits of detection.

We dated 274 fossil scleractinian corals from the three main target sites (Orphan Knoll, Nuuk, South Greenland) using a reconnaissance dating technique based on the decay of uranium to thorium (Spooner et al 2015, Chen et al 2015).

Foraminifera samples for stable isotope analysis were processed and analysed at the Lamont-Doherty Earth Observatory of Columbia University. Samples were freeze-dried and then washed through a 63 µm sieve and the >63 µm fraction dried at 45°C overnight. Five to ten specimens of *Neogloboquadrina pachyderma* (sinistral) were picked from the >250 µm size fraction, weighed to ensure consistent sample sizes and then analysed on a Thermo Delta V Plus with Kiel IV individual acid bath device. Values were calibrated to the VPDB isotope scale with NBS-19 and NBS-18. Reproducibility of the in-house standard (1SD) is ±0.06‰ for $\delta^{18}O$ and ±0.04‰ $\delta^{13}C$.

Ca and Sr intensities (count rates) were measured with an x-ray fluorescence (XRF) core scanner (ITRAX, Cox Ltd., Sweden) at the British Ocean Sediment Core Research Facility (BOSCORF). Split core surfaces were smoothed and covered with polypropylene film to minimize desiccation during analysis. Elemental counts were collected at 1 mm resolution, using an integration time of 2s and a molybdenum x-ray source set to 30kV and 30mA.

APPENDIX C: Supplementary figures

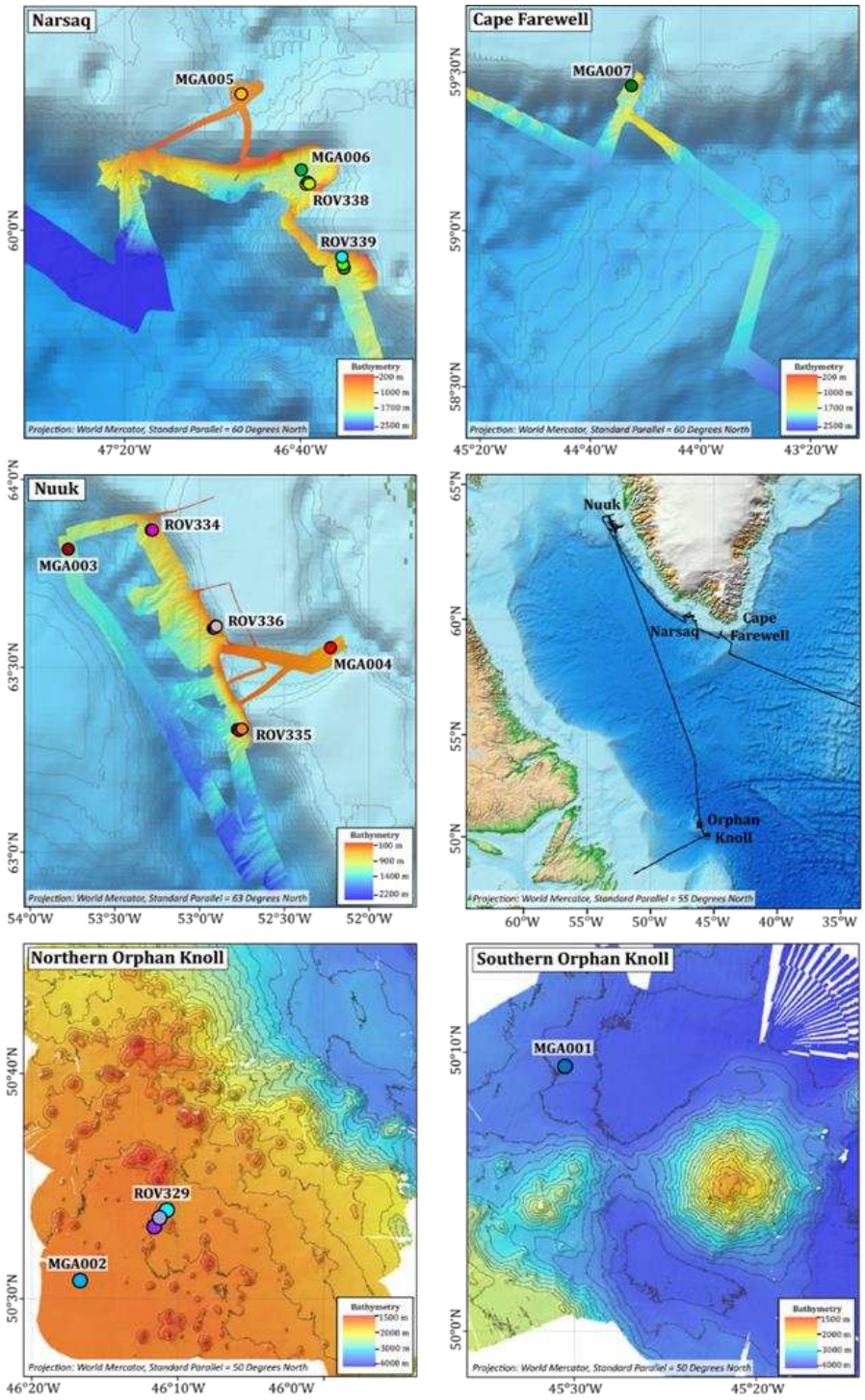

Figure A1. Maps showing DY081 mega core (MGA) and ROV push core sites where pore-fluid samples were taken, and cruise track (black line). Bathymetry resolution of the sampling regions were improved with shipboard multibeam survey. Circles marking the core locations have the same colours corresponding to those denoting the core identities in Figure 5.

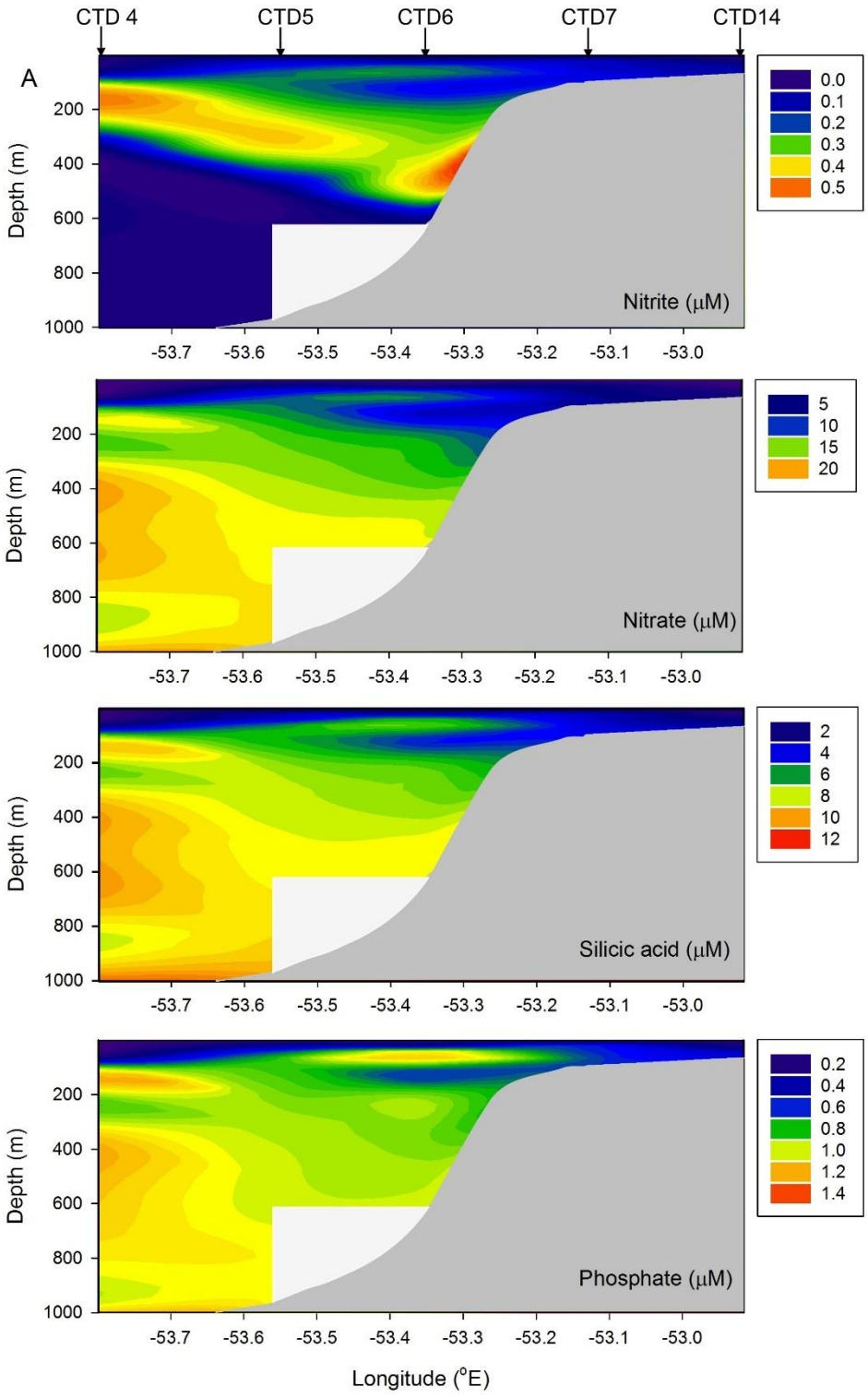

Figure A2: A) Example cross section of macronutrient concentrations from the northern section of the Nuuk grid (from CTD 4,5,6,7,14, see Figure 2), showing (from top to bottom): nitrite, nitrate+nitrite, silicic acid, and phosphate (all in μM). This section encompasses the margin from the slope onto the shelf, and did not occupy the bathymetric trough (c.f. Figure 3, main text).

866

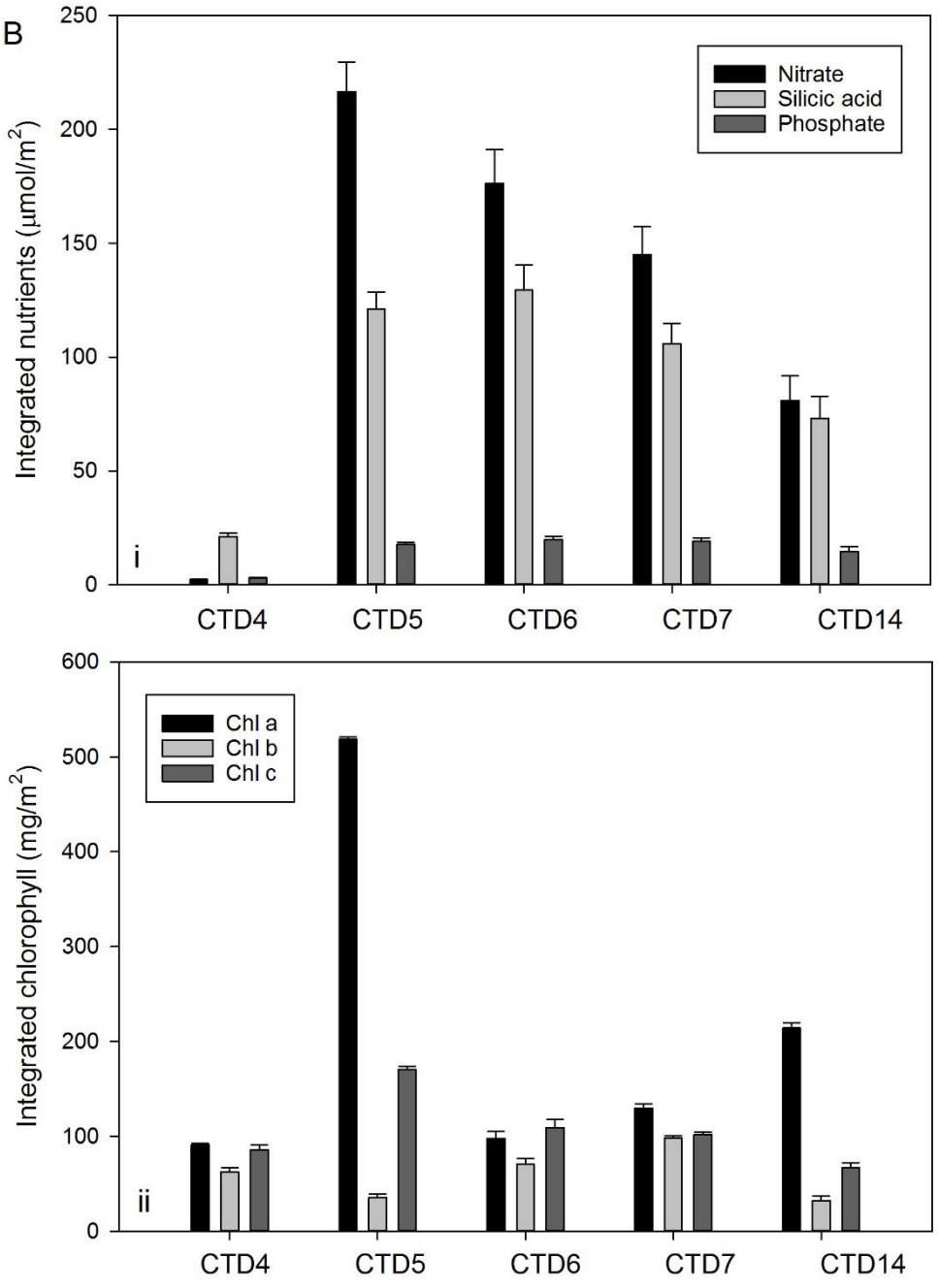

867

868 B) Example cross section of integrated (top 50m) macronutrient and algal pigment
869 concentrations from northern section of the Nuuk grid (from CTD 4 to CTD 7, 14, see Figure
870 2). i) Integrated macronutrients; ii) Integrated pigment concentrations. Error bars show
871 propagated errors on integration calculation (1SD).

872

873

874

A. Calculation one

Salinities set as per $d^{18}O$ mass balance (see main text)

Meteoric water alkalinity = 1000

Seawater alkalinity = 2312

Sea-ice alkalinity = 175

(Alkalinity in μmol/kg;

Data from Jones et al., 2008)

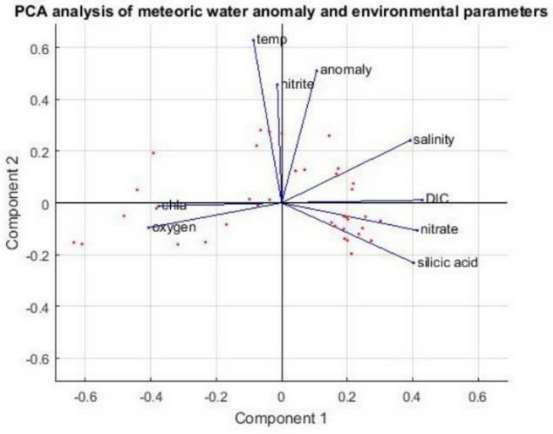

PC1 = 59%

PC2 = 17%

PC3 = 12%

Anomaly PC3 eigenvector <0.1

Anomaly = $\%Met_{d18O}$- $\%Met_{alk}$

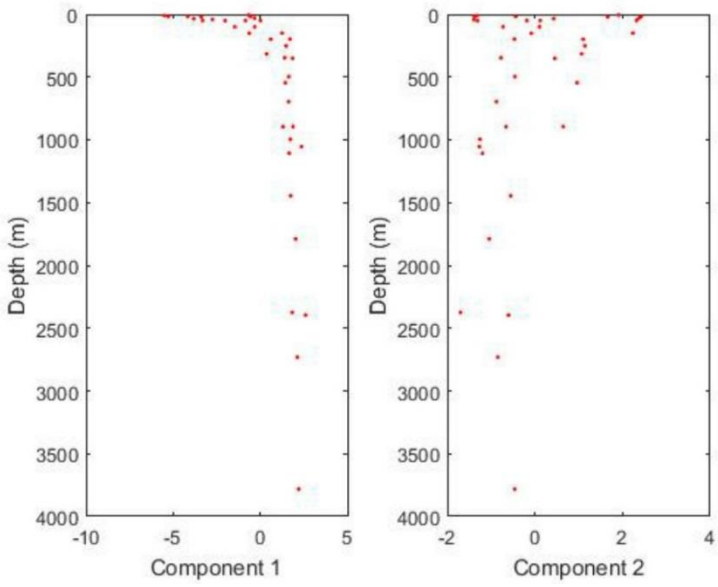

875

B. Calculation two

Salinities set as per d^{18}O mass balance (see main text)

Meteoric water alkalinity = 159
Seawater alkalinity = 2312
Sea-ice alkalinity = 175
(Alkalinity in μmol/kg;
Data from Meire et al., 2015;
Jones et al., 2008)

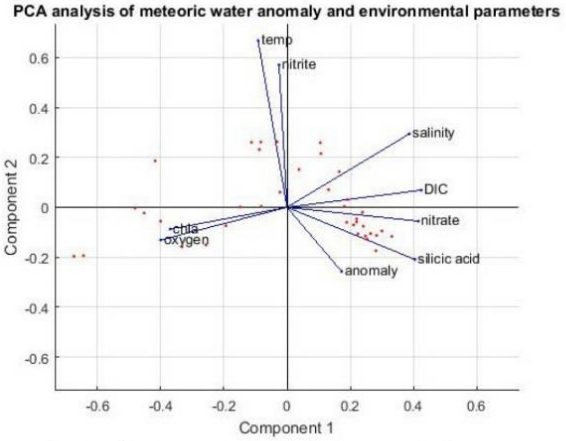

PC1 = 60%
PC2 = 15%
PC3 = 12%

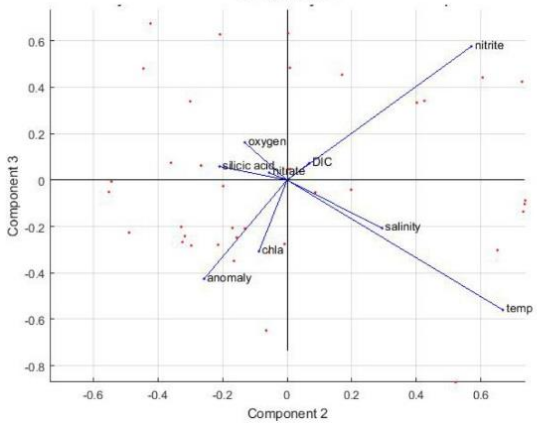

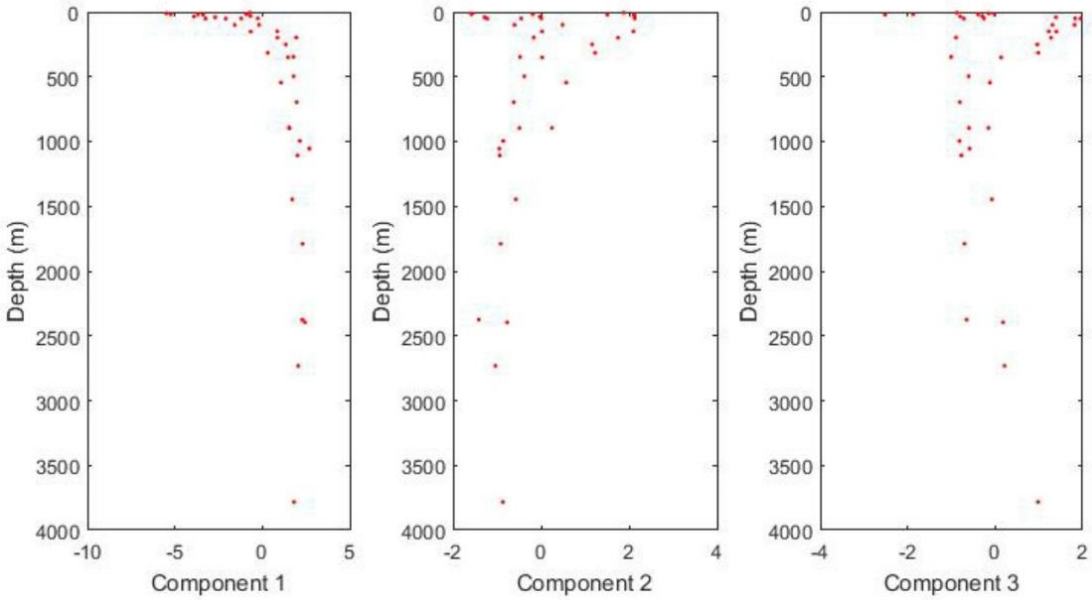

Figure A3: Comparison of different freshwater mass balance calculations. Mass balance calculations were carried out using i) salinity and seawater $\delta^{18}O$ (see main text, Table 1), and ii) salinity and total alkalinity (TA) measurements:

$$F_{ir} + F_{me} + F_{si} = 1$$

$$F_{ir}S_{ir} + F_{me}S_{me} + F_{si}S_{si} = S_{ms}$$

$$F_{ir}A_{ir} + F_{me}A_{me} + F_{si}A_{si} = A_{ms}$$

Where F_{ir}, F_{me}, F_{si} are the calculated fractions of Irminger Water, meteoric and sea ice melt respectively (Irminger Water being the chosen ocean endmember), which sum to 1 by definition. They result is clearly dependent on the exact choice of endmembers for salinity (S_{ir}, S_{me}, S_{si}) and TA (A_{ir}, A_{me}, A_{si}) for the Irminger Water, meteoric and sea ice melt respectively. S_{ms} and A_{ms} are the measured salinity and TA of each sample. Two different calculations were carried out using different end-members for meteoric water alkalinity: A) 1000 μmol/kg (typical value for the Arctic Ocean, from Jones et al., 2008), and B) 159 μmol/kg (glacial meltwater value from Meire et al., 2015). This latter value is more likely to be a robust representation of the end-member in this region compared to the High Arctic as glacial meltwater is likely to dominated meteoric inputs.

The anomaly between the percentage meteoric water was then calculated using:

$$\text{Anomaly} = \%\text{Met}_{\delta 18O} - \%\text{Met}_{alk}$$

Principal Component Analysis was then carried out comparing this anomaly with other environmental parameters. Component loadings (lines) and scores (dots) for the main axes are shown (top) together with depth profiles of scores (bottom). Note that the %Met anomalies show strong loading with axes that also show high scores at subsurface depths, and correlate well with nitrite concentrations and temperature. This suggests that the anomalies arise as a result of non-conservative behaviour perhaps associated with water column nitrification or sedimentary denitrification.

Additional references

Dickson, A.G., Sabine, C.L. and Christian, J.R., 2007. Guide to best practices for ocean CO2 measurements. North Pacific Marine Science Organization.

Hendry, K.R., 2017. RRS Discovery Cruise DY081, July 6th – August 8th 2017, National Marine Facilities.

Hendry, K.R. et al., 2018. Spatiotemporal Variability of Barium in Arctic Sea-Ice and Seawater. Journal of Geophysical Research: Oceans.

Henley, S.F. et al., 2018. Macronutrient and carbon supply, uptake and cycling across the Antarctic Peninsula shelf during summer. Phil. Trans. R. Soc. A, 376(2122): 20170168.

Hydes, D. et al., 2010. Recommendations for the determination of nutrients in seawater to high levels of precision and inter-comparability using continuous flow analysers. GO-SHIP (Unesco/IOC).

Krause, J.W., Brzezinski, M.A. and Jones, J.L., 2011. Application of low-level beta counting of 32Si for the measurement of silica production rates in aquatic environments. Marine Chemistry, 127(1-4): 40-47.

Kuzyk, Z.Z.A., Gobeil, C., Goñi, M.A. and Macdonald, R.W., 2017. Early diagenesis and trace element accumulation in North American Arctic margin sediments. Geochimica et Cosmochimica Acta, 203: 175-200.

Mackereth, F.J.H., Heron, J.t., Talling, J.F. and Association, F.B., 1978. Water analysis: some revised methods for limnologists.

McCartney, M., 1992. Recirculating components to the deep boundary current of the northern North Atlantic. Progress in Oceanography, 29(4): 283-383.

McCartney, M.S. and Talley, L.D., 1982. The subpolar mode water of the North Atlantic Ocean. Journal of Physical Oceanography, 12(11): 1169-1188.

Meredith, M.P. et al., 2008. Variability in the freshwater balance of northern Marguerite Bay, Antarctic Peninsula: results from $d^{18}O$. Deep-Sea Research II, 55: 309-322.

Sherrell, R.M., Annett, A.L., Fitzsimmons, J.N., Roccanova, V.J. and Meredith, M.P., 2018. A 'shallow bathtub ring'of local sedimentary iron input maintains the Palmer Deep biological hotspot on the West Antarctic Peninsula shelf. Phil. Trans. R. Soc. A, 376(2122): 20170171.

Thomas, H. et al., 2011. Barium and carbon fluxes in the Canadian Arctic Archipelago. Journal of Geophysical Research: Oceans, 116(C9).

Woodward, E. and Rees, A., 2001. Nutrient distributions in an anticyclonic eddy in the northeast Atlantic Ocean, with reference to nanomolar ammonium concentrations. Deep Sea Research Part II: Topical Studies in Oceanography, 48(4-5): 775-793.

942 Yang, Q. et al., 2016. Recent increases in Arctic freshwater flux affects Labrador Sea
943 convection and Atlantic overturning circulation. Nature communications, 7:
944 ncomms10525.

945
946

References

Alexeev, V.A., Walsh, J.E., Ivanov, V.V., Semenov, V.A., Smirnov, A.V., 2017. Warming in the Nordic Seas, North Atlantic storms and thinning Arctic sea ice. *Environmental Research Letters*, 12, 084011.

Andrews, J., Jennings, A.E., Kerwin, M., Kirby, M., Manley, W., Miller, G., Bond, G., MacLean, B., 1995. A Heinrich-like event, H-0 (DC-0): Source (s) for detrital carbonate in the North Atlantic during the Younger Dryas chronozone. *Paleoceanography*, 10, 943-952.

Andrews, J.T., Voelker, A.H., 2018. "Heinrich events"(& sediments): A history of terminology and recommendations for future usage. *Quaternary Science Reviews*, 187, 31-40.

Annett, A.L., Henley, S.F., Van Beek, P., Souhaut, M., Ganeshram, R., Venables, H.J., Meredith, M.P., Geibert, W., 2013. Use of radium isotopes to estimate mixing rates and trace sediment inputs to surface waters in northern Marguerite Bay, Antarctic Peninsula. *Antarct. Sci*, 25, 445-456.

Annett, A.L., Skiba, M., Henley, S.F., Venables, H.J., Meredith, M.P., Statham, P.J., Ganeshram, R.S., 2015. Comparative roles of upwelling and glacial iron sources in Ryder Bay, coastal western Antarctic Peninsula. *Marine Chemistry*, 176, 21-33.

Arrigo, K.R., van Dijken, G.L., Castelao, R.M., Luo, H., Rennermalm, Å.K., Tedesco, M., Mote, T.L., Oliver, H., Yager, P.L., 2017. Melting glaciers stimulate large summer phytoplankton blooms in southwest Greenland waters. *Geophysical Research Letters*, 44, 6278-6285.

Bamber, J., Tedstone, A., King, M., Howat, I., Enderlin, E., van den Broeke, M., Noel, B., 2018. Land ice freshwater budget of the Arctic and North Atlantic Oceans: 1. Data, methods, and results. *Journal of Geophysical Research: Oceans*, 123, 1827-1837.

Berthelsen, T., 2014. Coastal fisheries in Greenland. *KNAPK report, Nuuk*.

Bhatia, M.P., Kujawinski, E.B., Das, S.B., Breier, C.F., Henderson, P.B., Charette, M.A., 2013. Greenland meltwater as a significant and potentially bioavailable source of iron to the ocean. *Nature Geoscience*, 6, 274.

Biard, T., Krause, J.W., Stukel, M.R., Ohman, M.D., 2018. The Significance of giant Phaeodarians (Rhizaria) to Biogenic Silica Export in the California Current Ecosystem. *Global Biogeochemical Cycles*.

Biard, T., Stemmann, L., Picheral, M., Mayot, N., Vandromme, P., Hauss, H., Gorsky, G., Guidi, L., Kiko, R., Not, F., 2016. In situ imaging reveals the biomass of giant protists in the global ocean. *Nature*, 532, 504.

Bond, G., Broecker, W., Johnsen, S., McManus, J., Labeyrie, L., Jouzel, J., Bonani, G., 1993. Correlations between climate records from North Atlantic sediments and Greenland ice. *Nature*, 365, 143.

Bond, G., Heinrich, H., Broecker, W.S., Labeyrie, L.D., McManus, J., Andrews, J.E., Huon, S., Jantschik, R., Clasen, S., Simet, C., Tedesco, K., Klas, M., Bonani, G., Ivy, S., 1992. Evidence for massive discharges of icebergs into the North Atlantic ocean during the last glacial period. *Nature*, 360, 245-249.

Bond, G.C., Lotti, R., 1995. Iceberg discharges into the North Atlantic on millenial time scales during the last glaciation. *Science*, 267, 1005-1010.

Broecker, W.S., 2003. Does the trigger for abrupt climate change reside in the ocean or in the atmosphere? *Science*, 300, 1519-1522.

Broecker, W.S., Bond, G.C., Klas, M., Clark, E., McManus, J., 1992. Origin of the northern Atlantic's Heinrich events. *Climate Dynamics*, 6, 265-273.

Brzezinski, M.A., Krause, J.W., Church, M.J., Karl, D.M., Li, B., Jones, J.L., Updyke, B., 2011. The annual silica cycle of the North Pacific subtropical gyre. *Deep Sea Research Part I: Oceanographic Research Papers*, 58, 988-1001.

Cao, L., Fairbanks, R.G., Mortlock, R.A., Risk, M.J.J.Q.S.R., 2007. Radiocarbon reservoir age of high latitude North Atlantic surface water during the last deglacial. 26, 732-742.

Carmack, E.C., Yamamoto-Kawai, M., Haine, T.W., Bacon, S., Bluhm, B.A., Lique, C., Melling, H., Polyakov, I.V., Straneo, F., Timmermans, M.L., 2016. Freshwater and its role in the Arctic Marine System: Sources, disposition, storage, export, and physical and biogeochemical consequences in the Arctic and global oceans. *Journal of Geophysical Research: Biogeosciences*, 121, 675-717.

Chen, T., Robinson, L.F., Beasley, M.P., Claxton, L.M., Andersen, M.B., Gregoire, L.J., Wadham, J., Fornari, D.J., Harpp, K.S.J.S., 2016. Ocean mixing and ice-sheet control of seawater 234U/238U during the last deglaciation. 354, 626-629.

Clark, P.U., Pisias, N.G., Stocker, T.F., Weaver, A.J., 2002. The role of the thermohaline circulation in abrupt climate change. *Nature*, 415, 863.

Cuny, J., Rhines, P.B., Kwok, R., 2005. Davis Strait volume, freshwater and heat fluxes. *Deep Sea Research Part I: Oceanographic Research Papers*, 52, 519-542.

Cuny, J., Rhines, P.B., Niiler, P.P., Bacon, S., 2002. Labrador Sea boundary currents and the fate of the Irminger Sea Water. *Journal of Physical Oceanography*, 32, 627-647.

Dodd, P.A., Heywood, K.J., Meredith, M.P., Naveira-Garabato, A.C., Marca, A.D., Falkner, K.K., 2009. Sources and fate of freshwater exported in the East Greenland Current. *Geophysical Research Letters*, 36.

Dowdeswell, J.A., Canals, M., Jakobsson, M., Todd, B., Dowdeswell, E.K., Hogan, K., 2016. The variety and distribution of submarine glacial landforms and implications for ice-sheet reconstruction. *Geological Society, London, Memoirs*, 46, 519-552.

Egbert, G.D., Erofeeva, S.Y., 2002. Efficient inverse modeling of barotropic ocean tides. *Journal of Atmospheric and Oceanic Technology*, 19, 183-204.

Enderlin, E.M., Howat, I.M., Jeong, S., Noh, M.J., Van Angelen, J.H., Van Den Broeke, M.R., 2014. An improved mass budget for the Greenland ice sheet. *Geophysical Research Letters*, 41, 866-872.

Felikson, D., Bartholomaus, T.C., Catania, G.A., Korsgaard, N.J., Kjær, K.H., Morlighem, M., Noël, B., Van Den Broeke, M., Stearns, L.A., Shroyer, E.L., 2017. Inland thinning on the Greenland ice sheet controlled by outlet glacier geometry. *Nature Geoscience*, 10, 366.

Fennel, K., Wilkin, J., Previdi, M., Najjar, R., 2008. Denitrification effects on air-sea CO2 flux in the coastal ocean: Simulations for the northwest North Atlantic. *Geophysical Research Letters*, 35.

Grousset, F., Labeyrie, L., Sinko, J., Cremer, M., Bond, G., Duprat, J., Cortijo, E., Huon, S., 1993. Patterns of ice-rafted detritus in the glacial North Atlantic (40–55° N). *Paleoceanography*, 8, 175-192.

Hawkings, J., Wadham, J., Tranter, M., Telling, J., Bagshaw, E., Beaton, A., Simmons, S.L., Chandler, D., Tedstone, A., Nienow, P., 2016. The Greenland Ice Sheet as a hot spot of phosphorus weathering and export in the Arctic. *Global Biogeochemical Cycles*, 30, 191-210.

Hawkings, J.R., Hatton, J.E., Hendry, K.R., de Souza, G.F., Wadham, J.L., Ivanovic, R., Kohler, T.J., Stibal, M., Beaton, A., Lamarche-Gagnon, G., 2018. The silicon cycle impacted by past ice sheets. *Nature Communications*, 9, 3210.

Hawkings, J.R., Wadham, J.L., Benning, L.G., Hendry, K.R., Tranter, M., Tedstone, A., Nienow, P., Raiswell, R., 2017. Ice sheets as a missing source of silica to the polar oceans. *Nature Communications*, 8, 14198.
Hawkings, J.R., Wadham, J.L., Tranter, M., Raiswell, R., Benning, L.G., Statham, P.J., Tedstone, A., Nienow, P., Lee, K., Telling, J., 2014. Ice sheets as a significant source of highly reactive nanoparticulate iron to the oceans. *Nature Communications*, 5.
Heinrich, H., 1988. Origin and consequences of cyclic ice rafting in the northeast Atlantic Ocean during the past 130,000 years. *Quaternary Research*, 29, 142-152.
Hendry, K.R., 2017. RRS Discovery Cruise DY081, July 6th – August 8th 2017. National Marine Facilities.
Hendry, K.R., Pyle, K.M., Barney Butler, G., Cooper, A., Fransson, A., Chierici, M., Leng, M.J., Meyer, A., Dodd, P.A., 2018. Spatiotemporal Variability of Barium in Arctic Sea-Ice and Seawater. *Journal of Geophysical Research: Oceans*.
Henley, S.F., Jones, E.M., Venables, H.J., Meredith, M.P., Firing, Y.L., Dittrich, R., Heiser, S., Stefels, J., Dougans, J., 2018. Macronutrient and carbon supply, uptake and cycling across the Antarctic Peninsula shelf during summer. *Phil. Trans. R. Soc. A*, 376, 20170168.
Hillaire-Marcel, C., Bilodeau, G., 2000. Instabilities in the Labrador Sea water mass structure during the last climatic cycle. *Canadian Journal of Earth Sciences*, 37, 795-809.
Hillaire-Marcel, C., Maccali, J., Ménabréaz, L., Ghaleb, B., Blénet, A., Edinger, E., 2017. U-series vs 14C ages of deep-sea corals from the southern Labrador Sea: Sporadic development of corals and geochemical processes hampering estimation of ambient water ventilation ages. *EGU General Assembly Conference Abstracts*, Vol. 19 (p. 9126).
Hodell, D.A., Channell, J.E., Curtis, J.H., Romero, O.E., Röhl, U., 2008. Onset of "Hudson Strait" Heinrich events in the eastern North Atlantic at the end of the middle Pleistocene transition (~ 640 ka)? *Paleoceanography*, 23.
Hopwood, M.J., Bacon, S., Arendt, K., Connelly, D., Statham, P., 2015. Glacial meltwater from Greenland is not likely to be an important source of Fe to the North Atlantic. *Biogeochemistry*, 124, 1-11.
Hopwood, M.J., Carroll, D., Browning, T.J., Meire, L., Mortensen, J., Krisch, S., Achterberg, E.P., 2018. Non-linear response of summertime marine productivity to increased meltwater discharge around Greenland. *Nature Communications*, 9, 3256.
Jones, E., Anderson, L., Jutterström, S., Swift, J., 2008. Sources and distribution of fresh water in the East Greenland Current. *Progress in Oceanography*, 78, 37-44.
Katsman, C.A., Spall, M.A., Pickart, R.S., 2004. Boundary current eddies and their role in the restratification of the Labrador Sea. *Journal of Physical Oceanography*, 34, 1967-1983.
Kenchington, E., Yashayaev, I., Tendal, O.S., Jørgensbye, H., 2017. Water mass characteristics and associated fauna of a recently discovered Lophelia pertusa (Scleractinia: Anthozoa) reef in Greenlandic waters. *Polar Biology*, 40, 321-337.
Krause, J.W., Brzezinski, M.A., Jones, J.L., 2011. Application of low-level beta counting of 32Si for the measurement of silica production rates in aquatic environments. *Marine Chemistry*, 127, 40-47.
Krause, J.W., Duarte, C.M., Marquez, I.A., Assmy, P., Fernández-Méndez, M., Wiedmann, I., Wassmann, P., Kristiansen, S., Agustí, S., 2018. Biogenic silica production and diatom dynamics in the Svalbard region during spring. *Biogeosciences*, 15, 6503-6517.
Krause, J.W., Nelson, D.M., Lomas, M.W., 2010. Production, dissolution, accumulation, and potential export of biogenic silica in a Sargass Sea mode-water eddy. *Limnology and Oceanography*, 55, 569-579.

Krause, J.W., Schulz, I.K., Rowe, K.A., Dobbins, W., Winding, M., Sejr, M., Duarte, C.M., Agustí, S., In review. Silicon limitation drives bloom termination and carbon sequestration in an Arctic bloom. *Scientific reports*.

Kuzyk, Z.Z.A., Gobeil, C., Goñi, M.A., Macdonald, R.W., 2017. Early diagenesis and trace element accumulation in North American Arctic margin sediments. *Geochimica et Cosmochimica Acta*, 203, 175-200.

Lindsay, R., Schweiger, A., 2015. Arctic sea ice thickness loss determined using subsurface, aircraft, and satellite observations. *The Cryosphere*, 9, 269-283.

Luo, H., Castelao, R.M., Rennermalm, A.K., Tedesco, M., Bracco, A., Yager, P.L., Mote, T.L., 2016. Oceanic transport of surface meltwater from the southern Greenland ice sheet. *Nature Geoscience*, 9, 528.

Lynch-Stieglitz, J., Schmidt, M.W., Henry, L.G., Curry, W.B., Skinner, L.C., Mulitza, S., Zhang, R., Chang, P., 2014. Muted change in Atlantic overturning circulation over some glacial-aged Heinrich events. *Nature Geoscience*, 7, 144.

Maslanik, J., Fowler, C., Stroeve, J., Drobot, S., Zwally, J., Yi, D., Emery, W., 2007. A younger, thinner Arctic ice cover: Increased potential for rapid, extensive sea-ice loss. *Geophysical Research Letters*, 34.

McManus, J.F., Anderson, R.F., Broecker, W.S., Fleisher, M.Q., Higgins, S.M., 1998. Radiometrically determined sedimentary fluxes in the sub-polar North Atlantic during the last 140,000 years. *Earth and Planetary Science Letters*, 155, 29-43.

McManus, J.F., Francois, R., Gherardi, J.-M., Keigwin, L.D., Brown-Leger, S., 2004. Collapse and rapid resumption of Atlantic meridional circulation linked to deglacial climate changes. *Nature*, 428, 834-837.

Meire, L., Meire, P., Struyf, E., Krawczyk, D., Arendt, K., Yde, J., Juul Pedersen, T., Hopwood, M.J., Rysgaard, S., Meysman, F., 2016. High export of dissolved silica from the Greenland Ice Sheet. *Geophysical Research Letters*, 43, 9173-9182.

Meire, L., Mortensen, J., Meire, P., Juul-Pedersen, T., Sejr, M.K., Rysgaard, S., Nygaard, R., Huybrechts, P., Meysman, F.J., 2017. Marine-terminating glaciers sustain high productivity in Greenland fjords. *Global Change Biology*, 23, 5344-5357.

Meire, L., Søgaard, D., Mortensen, J., Meysman, F., Soetaert, K., Arendt, K., Juul-Pedersen, T., Blicher, M., Rysgaard, S., 2015. Glacial meltwater and primary production are drivers of strong CO2 uptake in fjord and coastal waters adjacent to the Greenland Ice Sheet. *Biogeosciences*, 12, 2347-2363.

Melling, H., Moore, R.M., 1995. Modification of halocline source waters during freezing on the Beaufort Sea shelf: evidence from oxygen isotopes and dissolved nutrients. *Continental Shelf Research*, 15, 89-113.

Meredith, M., Heywood, K., Dennis, P., Goldson, L., White, R., Fahrbach, E., Schauer, U., Østerhus, S., 2001. Freshwater fluxes through the western Fram Strait. *Geophysical Research Letters*, 28, 1615-1618.

Meredith, M.P., Brandon, M.A., Wallace, M.I., Clarke, A., Leng, M.J., Renfrew, I.A., van Lipzig, N.P.M., King, J.C., 2008. Variability in the freshwater balance of northern Marguerite Bay, Antarctic Peninsula: results from d^{18}O. *DEep-Sea Research II*, 55, 309-322.

Moore, W.S., 2008. Fifteen years experience in measuring 224Ra and 223Ra by delayed-coincidence counting. *Marine Chemistry*, 109, 188-197.

Moore, W.S., Arnold, R., 1996. Measurement of 223Ra and 224Ra in coastal waters using a delayed coincidence counter. *Journal of Geophysical Research: Oceans*, 101, 1321-1329.

1130 Moros, M., Kuijpers, A., Snowball, I., Lassen, S., Bäckström, D., Gingele, F., McManus,
1131 J.J.M.G., 2002. Were glacial iceberg surges in the North Atlantic triggered by climatic
1132 warming? , 192, 393-417.
1133 Moros, M., McManus, J., Rasmussen, T., Kuijpers, A., Dokken, T., Snowball, I., Nielsen, T.,
1134 Jansen, E., 2004. Quartz content and the quartz-to-plagioclase ratio determined by X-ray
1135 diffraction: a proxy for ice rafting in the northern North Atlantic? *Earth and Planetary*
1136 *Science Letters*, 218, 389-401.
1137 Myers, P.G., Donnelly, C., Ribergaard, M.H., 2009. Structure and variability of the West
1138 Greenland Current in Summer derived from 6 repeat standard sections. *Progress in*
1139 *Oceanography*, 80, 93-112.
1140 Nelson, D.M., Treguer, P., Brzezinski, M.A., Leynaert, A., Queguiner, B., 1995. Production
1141 and dissolution of biogenic silica in the ocean: revised global estimates, comparison with
1142 regional data and relationship to biogenic sedimentation. *Global Biogeochemical Cycles*, 9,
1143 359-372.
1144 Oliver, H., Luo, H., Castelao, R.M., van Dijken, G.L., Mattingly, K.S., Rosen, J.J., Mote, T.L.,
1145 Arrigo, K.R., Rennermalm, Å.K., Tedesco, M., 2018. Exploring the Potential Impact of
1146 Greenland Meltwater on Stratification, Photosynthetically Active Radiation, and Primary
1147 Production in the Labrador Sea. *Journal of Geophysical Research: Oceans*, 123, 2570-2591.
1148 Proshutinsky, A., Dukhovskoy, D., Timmermans, M.-L., Krishfield, R., Bamber, J.L., 2015.
1149 Arctic circulation regimes. *Phil. Trans. R. Soc. A*, 373, 20140160.
1150 Provost, C., Sennéchael, N., Miguet, J., Itkin, P., Rösel, A., Koenig, Z., Villacieros-Robineau,
1151 N., Granskog, M.A., 2017. Observations of flooding and snow-ice formation in a thinner
1152 Arctic sea ice regime during the N-ICE2015 campaign: Influence of basal ice melt and storms.
1153 *Journal of Geophysical Research: Oceans*.
1154 Ragueneau, O., Gallinari, M., Corrin, L., Grandel, S., Hall, P., Hauvespre, A., Lampitt, R.,
1155 Rickert, D., Stahl, H., Tengberg, A., 2001. The benthic silica cycle in the Northeast Atlantic:
1156 annual mass balance, seasonality, and importance of non-steady-state processes for the
1157 early diagenesis of biogenic opal in deep-sea sediments. *Progress in Oceanography*, 50, 171-
1158 200.
1159 Rahman, S., Aller, R., Cochran, J., 2017. The missing silica sink: revisiting the marine
1160 sedimentary Si cycle using cosmogenic 32Si. *Global Biogeochemical Cycles*.
1161 Rashid, H., Hesse, R., Piper, D.J., 2003. Evidence for an additional Heinrich event between H5
1162 and H6 in the Labrador Sea. *Paleoceanography*, 18.
1163 Robinson, L.F., Adkins, J.F., Frank, N., Gagnon, A.C., Prouty, N.G., Roark, E.B., van de Flierdt,
1164 T.J.D.S.R.P.I.T.S.i.O., 2014. The geochemistry of deep-sea coral skeletons: a review of vital
1165 effects and applications for palaeoceanography. 99, 184-198.
1166 Ruddiman, W.F., Sancetta, C., McIntryre, A., 1977. Glacial/interglacial response rate of
1167 subpolar North Atlantic waters to climatic change: the record in oceanic sediments. *Phil.*
1168 *Trans. R. Soc. Lond. B*, 280, 119-142.
1169 Ryan, J., Dowdeswell, J., Hogan, K., 2016. Three cross-shelf troughs on the continental shelf
1170 of SW Greenland from Olex data. *Geological Society, London, Memoirs*, 46, 167-168.
1171 Rykova, T., Straneo, F., Bower, A.S., 2015. Seasonal and interannual variability of the West
1172 Greenland Current System in the Labrador Sea in 1993–2008. *Journal of Geophysical*
1173 *Research: Oceans*, 120, 1318-1332.
1174 Schofield, O., Ducklow, H., Bernard, K., Doney, S., Patterson-Fraser, D., Gorman, K.,
1175 Martinson, D., Meredith, M., Saba, G., Stammerjohn, S., 2013. Penguin biogeography along

the West Antarctic Peninsula: Testing the canyon hypothesis with Palmer LTER observations. *Oceanography*, 26, 204-206.
Schulze, L.M., Frajka-Williams, E., 2018. Wind-driven transport of fresh shelf water into the upper 30m of the Labrador Sea. *Ocean Science*, 14(5), 1247-1264.
Sherrell, R.M., Annett, A.L., Fitzsimmons, J.N., Roccanova, V.J., Meredith, M.P., 2018. A 'shallow bathtub ring'of local sedimentary iron input maintains the Palmer Deep biological hotspot on the West Antarctic Peninsula shelf. *Phil. Trans. R. Soc. A*, 376, 20170171.
Stoner, J.S., Channell, J.E., Hillaire-Marcel, C., 1996. The magnetic signature of rapidly deposited detrital layers from the deep Labrador Sea: Relationship to North Atlantic Heinrich layers. *Paleoceanography and Paleoclimatology*, 11, 309-325.
Thomas, H., Shadwick, E., Dehairs, F., Lansard, B., Mucci, A., Navez, J., Gratton, Y., Prowe, F., Chierici, M., Fransson, A., 2011. Barium and carbon fluxes in the Canadian Arctic Archipelago. *Journal of Geophysical Research: Oceans*, 116.
Van As, D., Andersen, M.L., Petersen, D., Fettweis, X., Van Angelen, J.H., Lenaerts, J.T., Van Den Broeke, M.R., Lea, J.M., Bøggild, C.E., Ahlstrøm, A.P., 2014. Increasing meltwater discharge from the Nuuk region of the Greenland ice sheet and implications for mass balance (1960–2012). *Journal of Glaciology*, 60, 314-322.
van den Broeke, M., Box, J., Fettweis, X., Hanna, E., Noël, B., Tedesco, M., van As, D., van de Berg, W.J., van Kampenhout, L., 2017. Greenland ice sheet surface mass Loss: recent developments in observation and modeling. *Current Climate Change Reports*, 3, 345-356.
Wadham, J.L., Hawkings, J., Telling, J., Chandler, D., Alcock, J., Lawson, E., Kaur, P., Bagshaw, E., Tranter, M., Tedstone, A., 2016. Sources, cycling and export of nitrogen on the Greenland Ice Sheet. *Biogeosciences Discussions*.
Wang, Y.-J., Cheng, H., Edwards, R.L., An, Z., Wu, J., Shen, C.-C., Dorale, J.A., 2001. A high-resolution absolute-dated late Pleistocene monsoon record from Hulu Cave, China. *Science*, 294, 2345-2348.
Weatherdon, L.V., Magnan, A.K., Rogers, A.D., Sumaila, U.R., Cheung, W.W., 2016. Observed and projected impacts of climate change on marine fisheries, aquaculture, coastal tourism, and human health: an update. *Frontiers in Marine Science*, 3, 48.
Wolf-Gladrow, D.A., Zeebe, R.E., Klaas, C., Körtzinger, A., Dickson, A.G.J.M.C., 2007. Total alkalinity: The explicit conservative expression and its application to biogeochemical processes. 106, 287-300.
Yang, Q., Dixon, T.H., Myers, P.G., Bonin, J., Chambers, D., Van Den Broeke, M., Ribergaard, M.H., Mortensen, J., 2016. Recent increases in Arctic freshwater flux affects Labrador Sea convection and Atlantic overturning circulation. *Nature Communications*, 7, ncomms10525.